

H_0 tension or T_0 tension?

Mikhail M. Ivanov,^{1,2,*} Yacine Ali-Haïmoud,^{1,†} and Julien Lesgourgues^{3,‡}

¹*Center for Cosmology and Particle Physics, Department of Physics,
New York University, New York, NY 10003, USA*

²*Institute for Nuclear Research of the Russian Academy of Sciences,
60th October Anniversary Prospect, 7a, 117312 Moscow, Russia*

³*Institute for Theoretical Particle Physics and Cosmology (TTK)
RWTH Aachen University, D-52056 Aachen, Germany*

We study if the discrepancy between the local and cosmological measurements of the Hubble constant H_0 can be reformulated as a tension in the cosmic microwave background (CMB) monopole temperature T_0 . The latter is customarily fixed to the FIRAS best-fit value in CMB data analyses. Although this value was confirmed by several independent experiments, it is interesting to see how much parameter constraints depend on this prior. We first provide a detailed pedagogical description of the T_0 effects on cosmological observables. We show that the recombination history and transfer functions do not depend on T_0 , provided they are parametrized by the energy scale rather than redshift, and at fixed dark matter and baryon densities per CMB photon. Thus, T_0 is only a property of the observer, quantifying the amount of expansion between key cosmological events and today. As a consequence, the sole effect of T_0 on small-scale primary CMB anisotropies is through the angular diameter distance to the epoch of last scattering, resulting in a near-perfect degeneracy between T_0 and H_0 . This geometric degeneracy is partially lifted by the late-time integrated Sachs-Wolfe effect and CMB lensing. Still, Planck data alone is consistent with a broad region in the $H_0 - T_0$ plane, implying that removing the FIRAS prior on T_0 can make Planck and SH0ES less discrepant, without introducing new physics beyond Λ CDM. One may break the degeneracy by combining Planck with SH0ES, yielding an independent measurement of T_0 , which happens to be in 3σ tension with FIRAS. Therefore, the Hubble tension indeed can be recast into the T_0 tension. The agreement with FIRAS is restored when combining Planck with the baryon acoustic oscillation data instead of SH0ES. Thus, the tension between SH0ES and cosmological measurements of H_0 persists even if we discard the FIRAS T_0 prior.

1. INTRODUCTION AND SUMMARY

The disagreement between the value of the Hubble constant H_0 measured by different methods (the so-called “Hubble tension”) has recently become a hot topic in cosmology. On the one hand, local measurements using the Cepheid-calibrated supernovae [1, 2] and strong lensing time-delays [3] yield a number around 74 km/s/Mpc. On the other hand, the Planck cosmic microwave background radiation (CMB) data [4], various large-scale structure (LSS) probes [5–11], as well as the local measurements based on the inverse distance ladder technique [12, 13] favour independently of each other a value close to 68 km/s/Mpc. The Hubble tension might be the result

of unaccounted systematics¹ or a manifestation of new exotic physics (see Ref. [17] for a review). Therefore, it is imperative to scrutinize various choices made in the analysis of each dataset. One of such assumptions is the value of the CMB monopole temperature T_0 , which is typically fixed when fitting the Planck CMB likelihoods. The rationale behind this choice is that T_0 has been measured from a combination of the COBE/FIRAS data, molecular lines, and balloon-borne experiments with an outstanding precision [18, 19],

$$T_{0,\text{FIRAS}} = (2.72548 \pm 0.00057) \text{ K}. \quad (1)$$

For simplicity, we will call this measurement just “FIRAS”. Note that before FIRAS, T_0 had been measured

* mi1271@nyu.edu

† yah2@nyu.edu

‡ julien.lesgourgues@physik.rwth-aachen.de

¹ See, e.g. Ref. [14] in the context of the Cepheid-calibrated supernovae and Refs. [15, 16] for discussions regarding the strong lensing time delays.

already with good accuracy by COBRA [20], and that there exist other independent measurements of T_0 from the observation of carbon monoxide absorption lines in quasar spectra [21], all compatible with FIRAS.²

The effect of T_0 on CMB anisotropies was studied in Refs. [24–28]. These past studies have either focused on the impact of uncertainties in T_0 on cosmological parameters inferred from CMB anisotropy data [24–26], on combining current CMB anisotropy data with external datasets to measure T_0 [27], or on determining whether future CMB-anisotropy experiments might be able to measure T_0 [28]. In this paper, we show, for the first time, that T_0 can be measured from *current* CMB anisotropy data *alone*. We moreover study whether removing the FIRAS prior on T_0 can alleviate the Hubble tension. Since the monopole temperature can be seen as a proxy for the age of the Universe, just like H_0 , the two quantities should be nearly perfectly degenerate. Clearly, the CMB measurement of H_0 must be influenced by the T_0 prior. Naively, this offers a tempting way to resolve the Hubble tension without new physics and any additional parameters beyond those already contained in the base Λ CDM model.

Aiming at restoring the agreement between Planck and SH0ES, we have reanalyzed the final Planck 2018 data without fixing the CMB monopole temperature. As expected, we have found that the CMB data exhibit a clear $H_0 - T_0$ degeneracy. However, even in this extended model, the SH0ES measurement remains in substantial ($\sim 3\sigma$) tension with Planck. Thus, combining Planck and SH0ES gives an *independent measurement* of T_0 . This value happens to be in $\sim 3\sigma$ tension with the FIRAS measurement. However, one can break the geometric CMB degeneracy between T_0 and H_0 equally well with low-redshift baryon acoustic oscillation (BAO) data. This leads to a different measurement of T_0 that agrees with FIRAS, while being in $\sim 3\sigma$ tension with SH0ES.

Thus, interestingly, the Hubble tension between Planck+FIRAS and SH0ES can be fully reformulated as a T_0 tension between Planck+SH0ES and FIRAS. However, when BAO data is taken into account, the very good

agreement between the measurements of Planck, FIRAS and BAO suggests that, as long as the Λ CDM model is assumed, SH0ES is the outlier.³

Another goal of this paper is to clarify the physical effect of T_0 on cosmological observables. In past works [24, 25], T_0 was varied while keeping H_0 and the *current* energy densities of the baryons and dark matter ω_b and ω_{cdm} fixed. However, recombination physics and the early-time CMB anisotropies are fully determined by the baryon-to-photon and CDM-particles-to-photon ratios, which results in almost perfect degeneracies between $H_0, \omega_b, \omega_{cdm}$ and T_0 [28]. Thus, varying T_0 with fixed H_0, ω_{cdm} and ω_b is not very informative. Instead, we show that it is more physically meaningful to study the effect of T_0 while keeping the ratios ω_{cdm}/T_0^3 and ω_b/T_0^3 constant. With these parameters fixed, the *temperature* of recombination is fixed, and a change of T_0 *mostly* amounts to changing the angular diameter distance to the last scattering surface, thus the angle θ_s that it subtends, resulting in a strong degeneracy with H_0 . In addition, however, a change in T_0 at fixed θ_s changes the time elapsed since matter- Λ equality, thus the late integrated Sachs-Wolfe effect and gravitational lensing. Through these late-time effects, we show that one can extract a 4% measurement of T_0 from Planck data *alone*, contrasting with the standard lore that this could not be done without external datasets [27, 28].

The remainder of this paper is structured as follows. We start with the discussion of our datasets in Sec. 2. We give some theoretical background in Sec. 3, whereas Sec. 4 contains our main results. Finally, we draw conclusions in Sec. 5.

2. DATA

For CMB anisotropy data, we use the Planck baseline TTTEEE + lowE + lensing likelihood⁴ from the 2018

² It is worth mentioning that there are further prospects to re-measure T_0 with experiments aimed at CMB spectral distortions. In particular, PIXIE [22] would allow one to reduce the uncertainty of the T_0 measurement down to $\sigma(T_0) \sim 10^{-7}$ K [23], which is 3 orders of magnitude better than FIRAS.

³ Note that, in principle, H_0 can also be measured from T_0 in a model-independent way via the observation of the CMB monopole cooling [29].

⁴ We stick here to the naming conventions of the Planck collaboration, in which “TTTEEE + lowE” stands for high- ℓ TT, TE, EE data combined with low- ℓ TT, EE data; while lensing refers to the measurement of the lensing deflection spectrum based on 4-point correlation functions of CMB maps [4].

data release [4] as implemented in `Montepython v3.0` [30], see Ref. [31] for likelihood details. Since the standard recombination code `recfast` [32] uses fudge functions calibrated for a fixed T_0 , we use the more flexible and accurate code `HyRec` [33, 34] that does not rely on any fiducial cosmology. In addition to the cosmological parameters, we vary 21 Planck nuisance parameters that capture various instrumental and systematic effects [31].

As for the SH0ES data, we will use a Gaussian prior on H_0 derived from the most recent measurements by the SH0ES collaboration [2],

$$H_0 = 73.5 \pm 1.4 \text{ km/s/Mpc}. \quad (2)$$

Moreover, we will employ BAO data from the BOSS data release 12 [35]. In principle, one can derive better constraints from the full BOSS likelihood that includes the shape information as well [36]. However, the compressed likelihood involving only the BAO scale will be sufficient if our goal is to break geometric degeneracies (see Ref. [37] for a discussion on the role of the BOSS data in combination with Planck). In principle, one can also use more BAO measurements, e.g. from the Ly- α [38] and quasar data [39]. However, the single most constraining BAO dataset from BOSS DR12 will be enough for the purposes of our paper.

The CMB monopole temperature T_0 has already been constrained independently of FIRAS in the Planck 2015 analysis [27], which gave the following result from the combination of TT, TE, EE and BAO data,

$$T_0 = (2.718 \pm 0.021) \text{ K}. \quad (3)$$

In this paper, it was already pointed out that the Planck data have a strong geometric degeneracy between H_0 and T_0 , which can be broken by BAO measurements. In the next sections we will explain in detail the origin of this degeneracy, and show how it can also be broken by SH0ES.

3. THEORY BACKGROUND

3.1. Cosmological model and parameters

In this paper, we use geometric units $G = c = 1$. For short, we define the constant rate

$$\gamma_{100} \equiv \frac{H_0}{h} = 100 \text{ km/s/Mpc}. \quad (4)$$

In what follows we will focus on the Planck baseline Λ CDM model [4]. Specifically, we assume a spatially flat Universe with a cosmological constant $\Lambda = 8\pi\rho_\Lambda$, containing thermal photons at temperature T_γ , cold dark matter, non-relativistic baryons, two massless neutrinos and a single massive neutrino with minimal mass $m_\nu = 0.06 \text{ eV}$ (but our entire discussion would hold in the more realistic case of three non-zero masses). We assume that neutrinos have the standard temperature $T_\nu = (4/11)^{1/3}T_\gamma$, and that the small non-thermal distortions to their spectrum can be accounted for with an effective number of relativistic degrees of freedom $N_{\text{eff}} = 3.046$.

Moreover, we assume scalar adiabatic initial conditions characterized by a simple power-law power spectrum. The cosmological model is then entirely determined by 7 parameters:

- 2 parameters determining the initial conditions: the amplitude A_s at a reference scale $k_P = 0.05 \text{ Mpc}^{-1}$ and tilt n_s of the spectrum of primordial curvature fluctuations \mathcal{R} , $\Delta_{\mathcal{R}}^2 = A_s(k/k_P)^{n_s-1}$.
- 4 independent parameters determining the matter and energy content: the cosmological constant Λ , the present-time radiation temperature T_0 and the present-time baryon and cold dark matter densities $\rho_{b,0}, \rho_{c,0}$, or their dimensionless versions $\omega_i \equiv \frac{8\pi}{3}\rho_{i,0}/\gamma_{100}^2$. Instead of Λ , one can equivalently use the Hubble parameter H_0 or the angular scale θ_s of the sound horizon at last scattering. This phenomenological parameter is designed to approximate the observed angular scale of the CMB acoustic peaks.⁵
- 1 astrophysical parameter: the optical depth τ_{reio} to reionization.

3.2. How can we know whether T_0 is measurable?

It is standard in CMB anisotropy analyses to set T_0 to the mean value measured by FIRAS. Here we shall instead take T_0 as a free parameter. To check whether T_0 is actually measurable, we want to understand

⁵ By definition $\theta_s = r_s/((1+z_*)D_A(z_*))$ (r_s is the comoving sound horizon at the redshift of recombination z_* , $D_A(z_*)$ is the angular diameter distance to the last scattering surface). It should be borne in mind that this definition is somewhat ambiguous because recombination is not an instantaneous process.

whether the impact of a variation of T_0 on cosmological observables can be absorbed by a rescaling of other parameters. Such observables depend on the evolution of several quantities that can be expressed as a function of different measures of time: proper time t , conformal time η , redshift z , the scale factor $a = 1/(1+z)$, the energy scale, etc. We want to study whether we can “vary T_0 and other parameters while keeping the cosmological evolution unchanged”, but given the previous remark, this could have several different meanings. The most relevant options are:

(i) To maintain a fixed expansion history *relative to today*. This choice may also be sensible, because several observables depend on characteristic scales measured relatively to lengths today, and on the amount of expansion between characteristic times and today. For instance, the amplitude of matter perturbations at some redshift z relative to their amplitude today depends on the value of their wavelength relative to the Hubble radius today; the angle under which we see features in correlation functions depends on their size relative to the angular diameter distance, that we compute by integrating the expansion history relatively to the present time; the late integrated Sachs-Wolfe effect depends on the amount of expansion between matter-to- Λ equality and today; etc. To explore such a degeneracy, we should try to express all relevant quantities as a function of the redshift z (i.e. of the scale factor relative to today), and to show that if cosmological parameters are scaled properly when T_0 is varied, the quantities over which cosmological observables depend remain invariant. This could be achieved to some extent by fixing the parameter combinations ω_b/T_0^4 , ω_{cdm}/T_0^4 , Λ/T_0^4 , N_{eff} , etc.

(ii) To maintain cosmological evolution (of background, thermodynamics and perturbed quantities) as a function of *absolute energy scales*. This choice is motivated by the fact that important phenomena like nucleosynthesis or recombination are determined by absolute energy scales, such as particle masses, nuclear and atomic binding energies and energy levels, the neutron lifetime, etc. The most natural way to parametrize the energy scale is through the temperature of the thermal bath, T_γ . In this case, as we will see shortly, it is more meaningful to parametrize the baryon and dark matter densities by the following parameters, which are proportional to the

time-independent baryon-to-photon and dark matter-to-photon *number ratios*:

$$\varpi_i \equiv \frac{\omega_i}{T_0^3}, \quad i = b, c. \quad (5)$$

We also define $\varpi_m \equiv \varpi_b + \varpi_{cdm}$. As we will see, all cosmological quantities *at a given T_γ* depend on the parameters $\varpi_i, \Lambda, N_{\text{eff}}$, etc., but not *directly* on T_0 . This parametrization of the evolution of the Universe also requires redefining “comoving” scales as physical scales at a fixed *energy scale*, rather than a fixed time.

Of course, cosmological observables depend *both* on absolute energy scales and on the expansion history relative to today. Since the two scalings described above are incompatible with each other, a variation of T_0 cannot be fully absorbed. Thus the present photon temperature is indeed measurable with cosmological data, independently of FIRAS.

3.3. Background evolution and last scattering

We now show that, when expressing background quantities in terms of the photon temperature (rather than time t , redshift z or scale factor a), following the second scaling described in the previous section, they do not depend on T_0 , at fixed baryon-to-photon and CDM-to-photon number ratios ϖ_b, ϖ_{cdm} .

First, the Hubble rate $H(T_\gamma)$ is given by

$$H^2(T_\gamma) = \frac{\Lambda}{3} + \gamma_{100}^2 (\mathcal{A}(T_\gamma) T_\gamma^4 + \varpi_m T_\gamma^3), \quad (6)$$

where the function $\mathcal{A}(T_\gamma)$ is equal to a fixed number $\bar{\mathcal{A}}$ proportional to $1 + \frac{7}{8} \left(\frac{4}{11}\right)^{4/3} N_{\text{eff}}$ until the heaviest neutrino becomes non-relativistic, and later on only depends on the ratio⁶ m_ν/T_γ . Thus matter-radiation equality occurs at a temperature $T_{\text{eq}} = \varpi_m/\bar{\mathcal{A}}$ that only depends on ϖ_m . Of course, the *current* Hubble rate H_0 does depend on the current CMB temperature T_0 . Thus one can think of T_0 as parametrizing the current age of the Universe.

Second, in our baseline Λ CDM model, primordial nucleosynthesis starts with deuterium fusion, at a

⁶ or more realistically on $\sum_i m_{\nu i}/T_\gamma$, where the sum runs over all neutrinos that are non-relativistic at a given time.

temperature fixed by the baryon-to-photon number ratio and the deuterium binding energy. The final abundance of all primordial nuclei depends on nuclear rates and on the neutron-to-proton ratio, governed by the neutron lifetime, the effective number of degrees of freedom of the Standard Model, and the Fermi constant. Thus, in the minimal cosmological model, the only cosmological parameter relevant for this process is the baryon-to-photon number ratio, or equivalently ϖ_b . It sets in particular the primordial Helium fraction, Y_{He} , which is relevant for cosmological recombination⁷.

Lastly, cosmological recombination can formally be described by coupled equations of the form (see, e.g. [34])

$$\frac{dx_e}{dt} = \mathcal{F}(x_e, T_e, f_\nu, \rho_b, H, T_\gamma), \quad (7)$$

$$\frac{dT_e}{dt} = \mathcal{G}(x_e, T_e, H, T_\gamma), \quad (8)$$

$$\frac{df_\nu}{dt} = \mathcal{C}(x_e, f_\nu, \rho_b, H, T_\gamma), \quad (9)$$

where x_e is the free electron fraction, T_e is the electron temperature, f_ν is the photon phase-space density in the neighborhood of the Lyman- α transition, and the last equation is a Boltzmann equation describing its evolution. Upon rewriting these equations in terms of dx_e/dT_γ , dT_e/dT_γ , df_ν/dT_γ , and using the fact that $\rho_b \propto \varpi_b T_\gamma^3$ and H is a function of ϖ_m and T_γ only at the recombination epoch, we find that the free-electron fraction is a function of T_γ and $\varpi_b, \varpi_{\text{cdm}}$ only:

$$x_e = x_e(T_\gamma; \varpi_b, \varpi_{\text{cdm}}). \quad (10)$$

We show the free-electron fraction for different values of T_0 in Fig. 1, where we illustrate that, when keeping constant baryon-to-photon and dark matter-to-photon number ratios and expressing x_e as a function of T_γ , it is indeed independent of T_0 .

Given the recombination history $x_e(T_\gamma)$, one can compute the visibility function $g(\eta)$, which is the differential probability of last scattering per unit conformal time η :

$$g(\eta) \equiv \dot{\tau} \exp \left[- \int_\eta^{\eta_0} d\eta' \dot{\tau}(\eta') \right] \quad (11)$$

⁷ The CLASS code [40], that we will use in the following, includes a nucleosynthesis fitting function that adjusts Y_{He} as a function of ω_b , assuming the FIRAS value for T_0 . For the purpose of this work, we modified this fitting function, which now takes ϖ_b as its input parameter.

where $\dot{\tau} = an_{\text{H}}x_e\sigma_{\text{T}}$ is the differential Thomson optical depth, and η_0 is the current conformal time. It peaks at η_* such that $g'(\eta_*) = 0$, which thus solves the equation

$$\left. \frac{d\dot{\tau}}{d\eta} \right|_{\eta_*} = \dot{\tau}^2(\eta_*). \quad (12)$$

Rewriting $a = T_0/T_\gamma$ and using the fact that $n_{\text{H}}a^3$ is given by ω_b (up to a factor predicted by nucleosynthesis), we find that $\dot{\tau}/T_0$ is a function of $T_\gamma, \varpi_b, \varpi_{\text{cdm}}$. Using $d/d\eta = aHT_\gamma d/dT_\gamma = T_0Hd/dT_\gamma$, we then find that Eq. (12) is satisfied for a temperature $T_\gamma = T_*$ independent of T_0 , and depending only on $\varpi_b, \varpi_{\text{cdm}}$. For future reference, we write the corresponding fitting function that can be obtained by adjusting a numerical fit of Ref. [41],

$$T_* \approx 2970 \left(\frac{\varpi_m \text{ K}^3}{7.06 \times 10^{-3}} \right)^{0.0105} \left(\frac{\varpi_b \text{ K}^3}{1.1 \times 10^{-3}} \right)^{-0.028} \text{ K}. \quad (13)$$

Thus, the *temperature of last-scattering* T_* is independent of T_0 for some given $\varpi_b, \varpi_{\text{cdm}}$. Of course, the *redshift* of last-scattering z_* does depend on T_0 through $1 + z_* = T_*/T_0$, and so does the conformal time at last scattering $\eta_* \propto 1/T_0$.

The effective sound speed of the photon-baryon fluid $c_s = \frac{1}{\sqrt{3}} \left(1 + \frac{3}{4} \frac{\rho_b}{\rho_\gamma} \right)^{-1/2}$ is a function of T_γ, ϖ_b only. Therefore, the comoving sound horizon at last scattering r_s is such that $T_0 r_s$ is a function of $\varpi_b, \varpi_{\text{cdm}}$ only:

$$r_s = \int_0^{\eta_*} c_s d\eta = \frac{1}{T_0} \int_{T_*}^{\infty} c_s(T_\gamma; \varpi_b) \frac{dT_\gamma}{H(T_\gamma; \varpi_m)}. \quad (14)$$

This implies that the *physical scale* of the sound horizon at recombination, $a_* r_s = (T_0/T_*) r_s$, is a function of $\varpi_b, \varpi_{\text{cdm}}$ only, and does not depend on T_0 .

The same argument holds true for the moment of baryon decoupling (also called the baryon drag time), which happens slightly after recombination. Therefore, the physical size of the sound horizon at baryon decoupling $r_{d, \text{phys}}$, which is important for the BAO measurements, does not depend on T_0 . A useful fitting function for $r_{d, \text{phys}}$ can be obtained by combining Eq. (13) with the fit of Ref. [12],

$$r_{d, \text{phys}} = a_d r_d \approx 0.1386 \left(\frac{\varpi_m \text{ K}^3}{7.06 \times 10^{-3}} \right)^{-0.26} \times \left(\frac{\varpi_b \text{ K}^3}{1.10 \times 10^{-3}} \right)^{-0.10} \text{ Mpc}. \quad (15)$$

The CMB anisotropy power spectrum that we will discuss in 3.5 depends crucially on the physical photon diffusion

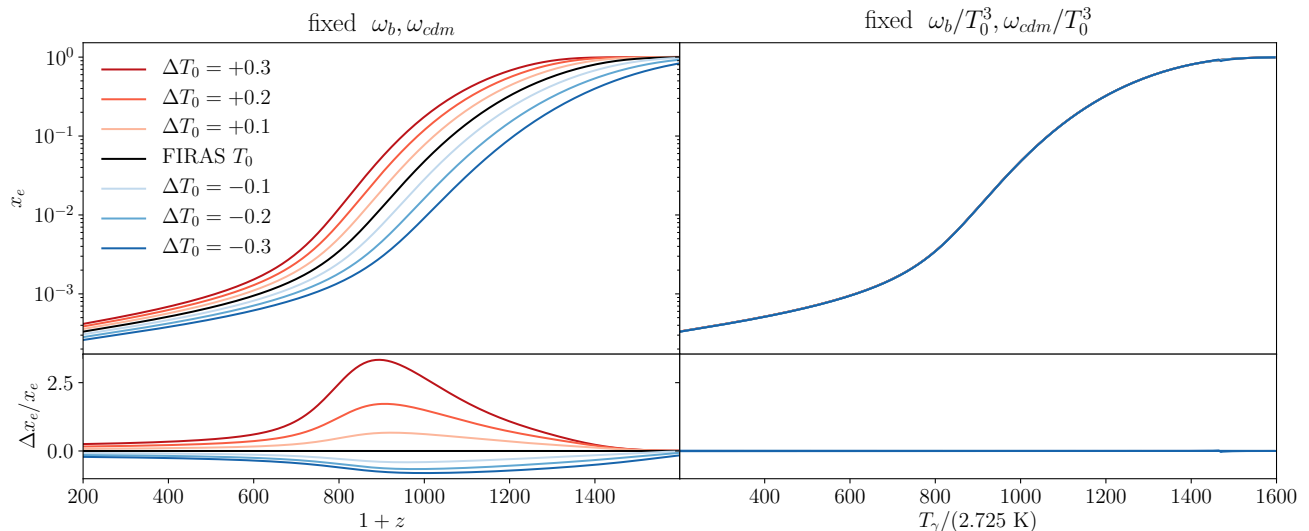


FIG. 1. Free-electron fraction x_e for different values of the present-day CMB monopole T_0 . On the left panel, we keep ω_b, ω_{cdm} constant, and show x_e as a function of redshift, which leads to large variations when changing T_0 , as found in Ref. [24]. On the right panel, we keep $\omega_b/T_0^3, \omega_{cdm}/T_0^3$ constant, and show x_e as a function of photon temperature. In terms of these rescaled variables, x_e is independent of T_0 . In both cases, the Helium mass fraction Y_{He} is kept constant; this is consistent with BBN predictions only if ω_b/T_0^3 is kept constant.

damping scale at last scattering, which is of the form

$$a_* r_{\text{damp}} = 2\pi \left[\int_0^{\eta_*} \frac{\mathcal{D}(R)}{\dot{\tau}} d\eta \right]^{1/2}, \quad (16)$$

where \mathcal{D} is a function of $R \equiv \frac{3\rho_b}{4\rho_\gamma}$ (see for instance [42]). Like for $a_* r_s$, some elementary steps show that this physical scale only depends on fundamental constants and on ϖ_b, ϖ_{cdm} .

3.4. Transfer functions and initial conditions

Transfer functions are solutions of the cosmological linear perturbation equations for each wavenumber k normalised in the super-Hubble regime, for instance, to $\mathcal{R}(k) = 1$. For fixed initial conditions, CMB anisotropy and large-scale structure observables depend on a number of such transfer functions evaluated at different epochs.

Another potential source of T_0 -dependence is the normalization of transfer functions. The cosmological perturbations are characterized by the conformal comoving wavenumber k , which is equal to the physical wavenumber now (which is typically normalized as $a = 1$ now). Since the current Universe age depends on T_0 , the comoving wavenumbers depend on it as well, as opposed to the *physical* wavenumbers. However, there is a way to

rescale the conformal momenta such that the dynamics of cosmological perturbations do not depend on T_0 .

It is a straightforward exercise to rewrite equations for linear cosmological perturbations in terms of T_γ rather than conformal time (starting from, e.g. [43]). By doing this, one can find that the transfer functions depend on $T_\gamma, \varpi_b, \varpi_{cdm}, \Lambda$ and k/T_0 , where k is the comoving wavenumber. This can be easily understood as follows. Instead of a set of comoving scales k that correspond to inverse physical scales at the current time, one can define another set of comoving scales \tilde{k} coinciding with inverse physical scales *at a fixed photon temperature*. If we choose arbitrarily this temperature to be $T_\gamma = 1$, the two sets are related through $\tilde{k} = k/T_0$.

Then, two universes with the same $\varpi_b, \varpi_{cdm}, \Lambda$ have the same \tilde{k} -dependent transfer functions *at a given photon temperature*. Such universes are statistically identical if they further have the same \tilde{k} -dependent power spectrum $\Delta_{\mathcal{R}}^2$ of scalar fluctuations. In other words, the r.m.s. amplitudes of primordial fluctuations should be the same on the same physical scales in both universes. The simple power-law spectrum motivated by inflation is typically defined at some arbitrary pivot scale k_P , which should be appropriately rescaled in a Universe with different T_0 . Alternatively, one could rescale the ampli-

tude itself. Indeed, keeping k_P fixed, we may rewrite the primordial curvature power spectrum as a function of $\tilde{k} = k/T_0$ as follows:

$$\Delta_{\mathcal{R}}^2 = A_s(k/k_P)^{n_s-1} = A_s T_0^{n_s-1} (\tilde{k}/k_P)^{n_s-1}. \quad (17)$$

Thus, in the case of power-law initial conditions, our scaling scheme requires the combination $A_s T_0^{n_s-1}$ to be fixed.

We illustrate these points in Fig. 2, where we show the matter power spectrum for several values of T_0 , but fixed ϖ_b, ϖ_c and $A_s T_0^{n_s-1}$, as a function of $\tilde{k} = k/T_0$. We see that it remains completely unaffected by T_0 when computed at the decoupling redshift z_{dec} , corresponding to the fixed energy scale T_* . However, when computing it *at the present time*, i.e. at an energy scale T_0 , its amplitude clearly varies with T_0 , as expected.

The value of the cosmological constant used to produce these plots is extracted from θ_s , which is fixed to the Planck best-fit value. This way, varying T_0 changes the amount of time elapsed since recombination until today, which changes the relative current fraction of the cosmological constant energy density w.r.t matter density. This leads to a different growth history and hence affects the amplitude of the power spectrum at $z = 0$. These effects will be discussed in detail momentarily.

3.5. Primary CMB anisotropies

There are two different contributions to the CMB primary (unlensed) power spectra. On small scales, anisotropies are mostly sourced by photon, baryon and metric fluctuations at last scattering, whose transfer functions contain damped oscillatory features associated to the physical sound horizon scale $a_* r_s$ and damping scale $a_* r_{\text{damp}}$. On large scales, the temperature spectrum receives an additional contribution from the late-time integrated Sachs-Wolfe (ISW) effect (see e.g. [44]), resulting from the time variation of gravitational potentials when the cosmological constant becomes important.

We have seen that for fixed $\varpi_b, \varpi_{\text{cdm}}, \Lambda$ and $A_s T_0^{n_s-1}$, not only the background evolution $H(T_\gamma)$ is independent of T_0 , but so are the temperature of last scattering T_* , the transfer functions expressed in terms of (T_γ, \tilde{k}) , and all r.m.s. fluctuations as a function of the same two variables. Nevertheless, the unlensed CMB spectra still depend on T_0 , for the two following reasons:

1. The CMB spectra are inferred from spherical maps, and thus expanded in multipoles rather than wavenumbers. The (Legendre) transformation from wavenumber to multipole space involves implicitly the angular diameter distance D_A , which contains an integral over the expansion history relative to the current time, and thus depends on T_0 , as anticipated in 3.2. For instance, the angular diameter distance to the last scattering surface reads

$$D_A(T_*) = a_* \int_{T_0}^{T_*} \frac{dT_\gamma}{T_0 H(T_\gamma)} = \frac{1}{T_*} \int_{T_0}^{T_*} \frac{dT_\gamma}{H(T_\gamma)}, \quad (18)$$

and depends explicitly on T_0 through the lower integration boundary. This means that the scaling that we discussed so far preserves the exact shape of the CMB unlensed spectra C_ℓ , on all scales for the polarization spectrum, and on small scales that are unaffected by the late ISW effect for the temperature spectrum. However it shifts these spectra horizontally to larger or smaller multipoles depending on the value of T_0 .

2. The late ISW effect depends essentially on the amount of expansion during Λ domination, given by $1 + z_\Lambda = T_\gamma^\Lambda / T_0$. For a fixed Λ , the photon temperature at matter-to- Λ equality T_γ^Λ is fixed, but z_Λ depends explicitly on T_0 . Thus late ISW contribution to the large scale temperature spectrum depends on T_0 .

We show the variations of CMB power spectra in Fig. 3 with different T_0 . On the left column, we keep $\omega_b, \omega_{\text{cdm}}, H_0$ and A_s constant, recovering the results of Refs. [24, 25]. On the right, we keep $\omega_b/T_0^3, \omega_{\text{cdm}}/T_0^3$ and $A_s T_0^{n_s-1}$ constant; we moreover keep the angular scale $\theta_s \equiv a_* r_s / D_A(T_*)$ fixed. The CLASS code [40] automatically adjusts Λ – or equivalently, $H_0 \simeq [\frac{\Lambda}{3} + \gamma_{100}^2 \varpi_m T_0^3]^{1/2}$ – to produce any requested input θ_s . We see that when these parameters are kept fixed, the TT, TE, and EE CMB spectra computed by the CLASS code [40] are exactly invariant on small scales when T_0 varies. However, this transformation preserves neither $(\Lambda, T_\gamma^\Lambda)$ and the absolute energy scale of Λ domination, nor $(\Omega_\Lambda, z_\Lambda)$ and the amount of expansion during Λ domination. Thus the amplitude of the late ISW effect is different, which can be seen as residual variations on large angular scales in Fig. 3. These large scales are poorly constrained by observations due to the effect of cosmic

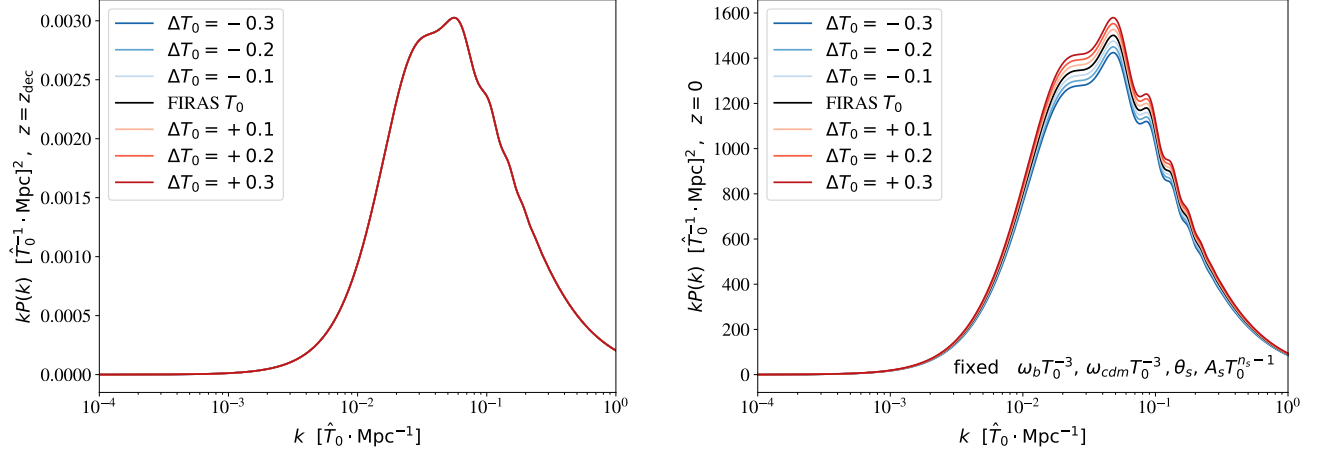


FIG. 2. Effect of a variation of T_0 (quoted in Kelvins) on the matter power spectrum at the time of last scattering (left panel) and today (right panel). The combinations ω_b/T_0^3 , ω_{cdm}/T_0^3 , θ_s and $A_s T_0^{n_s-1}$ are kept constant. In this case, the matter power spectrum computed at the time of last scattering (left panel) is independent of T_0 . A constant θ_s fixes the ratio between T_0 and Λ . This choice does not noticeably affect the physics at recombination, but introduces a correlation between T_0 and the growth factor seen when we evaluate the power spectrum at the present time (right panel). We use the units $\hat{T}_0 \cdot \text{Mpc}^{-1}$ ($\hat{T}_0 \equiv T_0/T_{0,\text{FIRAS}}$), such that all spectra are shown as functions of the same rescaled wavevector $\tilde{k} = k/T_0$.

variance. As a consequence, the large geometric degeneracy between T_0 and H_0 prevents CMB observations alone from providing tight bounds on either parameter.

We can understand the direction of the $T_0 - H_0$ degeneracy analytically as follows. The integral in eq. (18) is dominated by the low-temperature end, for which we may neglect the radiation contribution to $H(T_\gamma)$, i.e.

$$H(T_\gamma) \approx \gamma_{100} \sqrt{h^2 + \varpi_m(T_\gamma^3 - T_0^3)}. \quad (19)$$

Since $T_* \gg T_0$, we may further take the upper boundary to infinity, and arrive at

$$\begin{aligned} \gamma_{100} D_A(T_*) &\approx \frac{1}{T_*} \int_{T_0}^{\infty} \frac{dT}{\sqrt{h^2 + \varpi_m(T^3 - T_0^3)}} \\ &= \frac{T_0}{hT_*} \int_1^{\infty} \frac{dx}{\sqrt{1 + \Omega_m(x^3 - 1)}} \equiv \frac{T_0}{hT_*} \mathcal{I}(\Omega_m), \end{aligned} \quad (20)$$

where $\Omega_m \equiv \varpi_m T_0^3/h^2 = \omega_m/h^2$ is the usual matter density fraction, and the function $\mathcal{I}(\Omega_m)$ can be written in terms of a hypergeometric function.

Assuming the Planck+FIRAS best-fit values for ϖ_m , T_0 and h for numerical calculations, we obtain,

$$\left. \frac{\partial \ln D_A}{\partial \ln T_0} \right|_{\text{Planck}} \approx -0.22, \quad \left. \frac{\partial \ln D_A}{\partial \ln h} \right|_{\text{Planck}} \approx -0.19, \quad (21)$$

at constant ϖ_m . Thus, around the Planck best-fit cosmology, the angular diameter distance is mostly a function of the combination $H_0 T_0^{1.2}$, and we expect an approximate degeneracy $H_0 \propto T_0^{-1.2}$ at fixed ϖ_b, ϖ_{cdm} . This estimates agrees with the degeneracy found in our MCMC analysis for small variations of T_0 and H_0 around the baseline Planck cosmology. To capture larger deviations, we can use the exact implicit relation

$$\theta_s(H_0, T_0) \Big|_{\text{fixed } \varpi_b, \varpi_m} = \theta_{s, \text{best-fit Planck}}, \quad (22)$$

with θ_s being computed numerically in CLASS. This prediction for the degeneracy direction agrees well with the shape of our MCMC contours for the full range of T_0 and H_0 probed in the analysis, see Fig. 5. The details of this analysis will be discussed in the next Section.

3.6. CMB lensing

We have already seen that keeping ω_b/T_0^3 , ω_m/T_0^3 and θ_s constant does not preserve the amount of expansion taking place between last scattering and matter-to- Λ equality, given by T_*/T_γ^Λ , nor during Λ domination, given by T_γ^Λ/T_0 (where T_γ^Λ depends on T_0). A different ratio T_γ^Λ/T_0 implies a different amplitude of the late ISW contribution to large-scale temperature anisotropies. The

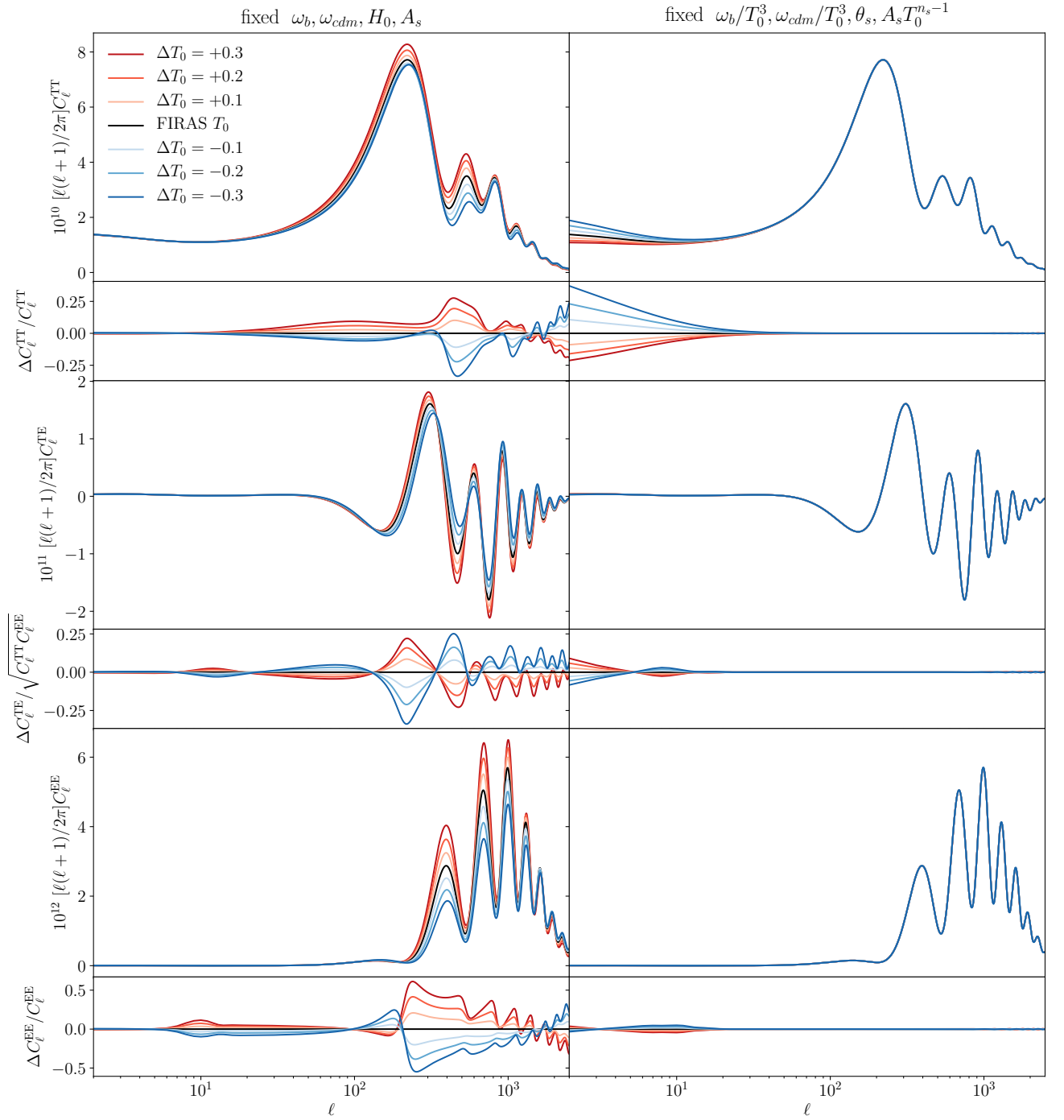


FIG. 3. Effect of a variation of T_0 (quoted in Kelvins) on the lensed TT, TE and EE CMB power spectra. In the left column, $\omega_b, \omega_{cdm}, H_0$ and A_s are kept constant, as in Refs. [24, 25]. In the right column, the combinations $\omega_b/T_0^3, \omega_{cdm}/T_0^3, \theta_s$ and $A_s T_0^{n_s-1}$ are kept constant. With the latter choice of constant parameters, CMB power spectra are independent of T_0 on small scales, but do depend on T_0 at large scales through the ISW effect. In both cases, τ_{reio} is kept constant.

variation of T_0 should be further imprinted through the CMB lensing effect, which also correlates with the late-time decay factor of metric fluctuations during Λ dom-

ination. Besides, the CMB lensing spectrum should be shifted horizontally by a different angular diameter distance to small redshifts. As is usually the case when

changing the redshift of matter-to- Λ equality, these different effects nearly compensate each other at the level of the lensing potential on small angular scales, and appear mainly at $\ell \lesssim 100$ [45]. This is confirmed in Fig. 4, where we show the power spectrum of deflection angle for different values of T_0 .

The smoothing of acoustic peaks in the CMB temperature and polarization spectra is sensitive to a broad range of multipoles around the peak of the deflection-angle power spectrum C_ℓ^{dd} shown in Fig. 4. Thus, this smoothing is slightly impacted by a change of T_0 when ω_b/T_0^3 , ω_{cdm}/T_0^3 , θ_s and $A_s T_0^{n_s-1}$ are kept constant. Together with the late ISW effect, this is one of the two mechanisms through which the (lensed) CMB spectra are sensitive to T_0 . Finally, CMB lensing extraction allows to measure the deflection spectrum and can marginally increase the sensitivity of CMB experiments to T_0 , although this technique has more sensitivity to scales $\ell \geq 70$ at which the effect of the CMB temperature on C_ℓ^{dd} is gradually suppressed.

In conclusion, we see that the geometric degeneracy of T_0 and H_0 in primary CMB anisotropies is broken by the ISW effect on large scales, as well as gravitational lensing. Actually, it gets broken even more clearly when including information on large scale structure observables, as we shall now discuss.

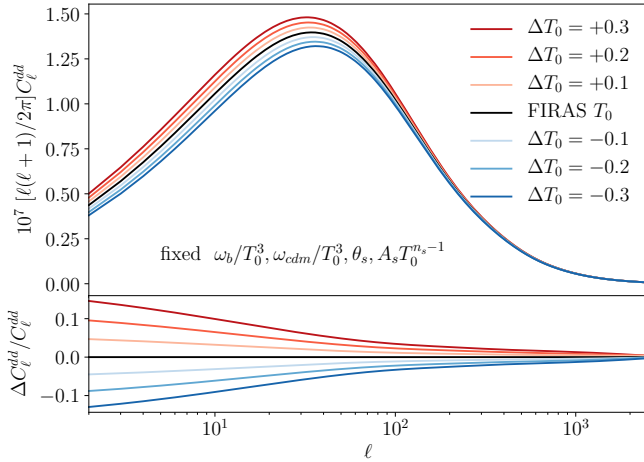


FIG. 4. Power spectrum of the lensing deflection angle as a function of T_0 , for fixed ω_b/T_0^3 , ω_c/T_0^3 , θ_s and $A_s T_0^{n_s-1}$. Note that this power spectrum is computed entirely within the Limber approximation for simplicity.

3.7. Large-scale structure

Let us discuss now the impact of varying T_0 on large-scale structure. For simplicity, let us focus on the baryon acoustic oscillation (BAO) measurements, which are widely used to break the geometric degeneracy of CMB data.

The galaxy distribution mapped by spectroscopic surveys is a three-dimensional observable, which is characterized by angles and redshifts. This can be contrasted with the CMB, whose BAO pattern is only observed in projection onto the two-dimensional last-scattering sphere.

The galactic BAO is usually probed through the position-space two-point correlation function, which peaks at the spatial separation corresponding to the physical size of the BAO scale at the observed epoch. This scale is not directly observed, because a galaxy survey only measures the angular position of the galaxies and their redshift. To convert these coordinates into a grid of comoving distances one typically assumes some fiducial cosmology. As long as the difference between the distances in fiducial and true cosmologies are small, the geodesic distance between a pair of galaxies can be described by the so-called Alcock-Paczynski (AP) scaling parameters⁸,

$$\alpha_{\parallel} = \frac{H_{\text{fid}}(z)}{H(z)}, \quad \alpha_{\perp} = \frac{D_A(z)}{D_{A,\text{fid}}(z)}. \quad (23)$$

α_{\parallel} and α_{\perp} capture, correspondingly, the radial and angular fractions of the separation between two galaxies. The description in terms of the AP parameters is adequate for space-times with small spatial curvature gradients that behave globally like the Friedman-Robertson-Walker-Lemaître Universe [49–51]. Thus, it will be sufficient for our analysis within the flat Λ CDM model.

The isotropic component of the galaxy distribution is mostly sensitive to the following combination of the AP parameters:

$$\alpha = (\alpha_{\parallel} \alpha_{\perp}^2)^{1/3}, \quad (24)$$

which describes how a small spatial volume “reconstructed” from the observed volume of angles and red-

⁸ See the original paper [46] and Refs. [47, 48] for the first applications of the scaling parameters in the form used nowadays, e.g. in the official BOSS data analysis [35].

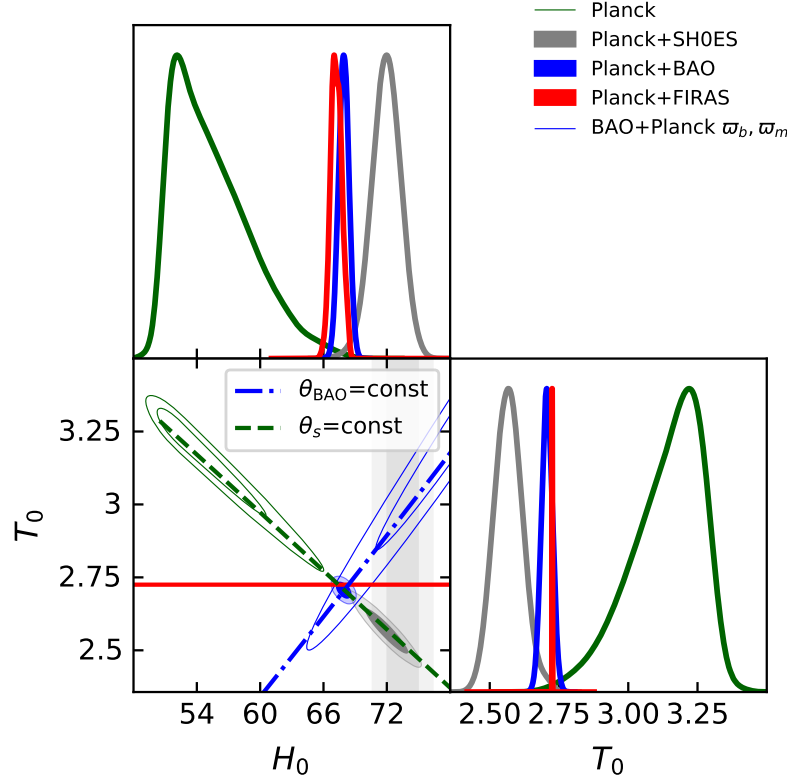


FIG. 5. Posterior distribution for T_0 and H_0 extracted from the analysis of the following data sets: Planck 2018 data, Planck plus the SH0ES H_0 prior, Planck plus the BOSS DR12 BAO, Planck plus the FIRAS T_0 prior, and finally the BAO plus the Planck priors on ω_b, ω_m . We stress that T_0 was varied in all these analyses. A horizontal solid red line marking the FIRAS value is put for illustrative purposes. The green dashed line shows the degeneracy direction $\theta_s(H_0, T_0) = \text{const}$ (which can be approximated as $H_0 \propto T_0^{-1.2}$ in the vicinity of the Planck+FIRAS best-fitting point), whereas the blue long dashed line shows the degeneracy $H_0 \propto T_0^{0.86}$ expected to produce a fixed BAO acoustic angle θ_{BAO} (see the main text for more details).

shifts rescales due to a difference between the true and fiducial cosmologies.

It is customary to parametrize the galactic BAO with an effective angular size of the acoustic peak in the two-point correlation function [44],

$$\theta_{\text{BAO}} = \frac{r_d}{D_V(z_{\text{eff}})}, \quad (25)$$

where z_{eff} is the effective (weighted) redshift (see e.g. Eq. (9) from Ref. [52]) and D_V is the effective comoving volume-averaged distance to the galaxy sample [49],

$$D_V(z_{\text{eff}}) = ((1 + z_{\text{eff}})^2 D_A^2(z_{\text{eff}}) z_{\text{eff}} / H(z_{\text{eff}}))^{1/3}. \quad (26)$$

Physically, θ_{BAO} can be thought of as a scale of the BAO in the angular two-point galaxy correlation function, which is averaged over the redshift bin of a survey. It is a very close counterpart of θ_s measured in the CMB

data. We stress that the AP conversion is only a technical tool to extract this angle from the data.⁹

The anisotropic part of the galaxy BAO signal is characterized by another combination of the AP parameters,

$$\epsilon = \left(\frac{\alpha_{\parallel}}{\alpha_{\perp}} \right)^{1/3} - 1, \quad (27)$$

which describes how the difference between the true and fiducial cosmology affects the relative scaling between the radial and transverse distances. The combination

⁹ Mathematically, it is equivalent to extracting the BAO scale from the angular power spectrum of the observed galaxies, as it is done for the CMB. An advantage of the distance conversion approach is that it allows one to directly compare the data to a 3d power spectrum model without having to project it onto the sky. A discussion on this point can be found, e.g. in Ref. [53].

of isotropic and anisotropic BAO signals allows one to separately constrain the parameters

$$\theta_{\text{BAO}, \parallel} \equiv r_d H(z_{\text{eff}}) \quad \text{and} \quad \theta_{\text{BAO}, \perp} \equiv \frac{r_d}{(1 + z_{\text{eff}}) D_A(z_{\text{eff}})}. \quad (28)$$

Note that the anisotropic BAO signal is a quite weak probe of cosmological parameters in minimal models [8, 46, 48]. The base Λ CDM model with varied CMB temperature T_0 considered in this paper also belongs to this class.

Importantly, the effective redshift of a galaxy sample z_{eff} is always known because it is measured directly from the data. This should be contrasted with the CMB observations. If the physical sound horizon at decoupling $r_{d, \text{phys}}$ is fixed, its comoving size depends on the unknown decoupling redshift z_{dec} and hence T_0 ,

$$r_d = r_{d, \text{phys}} \Big|_{z_{\text{dec}}} (1 + z_{\text{dec}}). \quad (29)$$

The effective volume-averaged distance to the galaxies has a different dependence on cosmological parameters compared to $D_A(z_*)$. Indeed, performing a calculation similar to Eq. (21) we find¹⁰

$$\frac{\partial \ln D_V}{\partial \ln H_0} \Big|_{z_{\text{eff}}=0.38} = -0.78, \quad \frac{\partial \ln D_V}{\partial \ln T_0} \Big|_{z_{\text{eff}}=0.38} = -0.33. \quad (30)$$

Combining it with Eq. (15) we obtain

$$\frac{\partial \ln \theta_{\text{BAO}}}{\partial \ln H_0} \Big|_{z_{\text{eff}}=0.38} = 0.78, \quad \frac{\partial \ln \theta_{\text{BAO}}}{\partial \ln T_0} \Big|_{z_{\text{eff}}=0.38} = -0.67. \quad (31)$$

Thus, the BAO angle θ_{BAO} constrains the combination $H_0 T_0^{-0.86}$, which is quite orthogonal to the line of constant $H_0 T_0^{1.2}$ probed by the CMB. This allows one to break the degeneracy between T_0 and H_0 when the galaxy BAO is combined with Planck.

This effect is illustrated in Fig. 5, where we show the $H_0 - T_0$ posterior extracted from the BOSS DR12 BAO data [39]. To obtain this posterior, we have fitted the BAO data with *minimal priors* from Planck 2018 data, namely the baryon- and matter-to-photon ratios ϖ_b, ϖ_m . The use of these priors is motivated by the following argument. When we eventually combine BAO and Planck 2018, the ϖ_b, ϖ_m limits will be totally dominated by

Planck, because they are measured to 1% precision from the shape of the CMB spectra independently of the late-time geometric expansion.

In passing, it is worth noting that the anisotropic BAO signal, in principle, allows one to separately measure T_0 and H_0 from the BAO data alone if the priors on ϖ_b, ϖ_m are imposed. Indeed, the full BAO signal is summarized in terms of two parameters, $r_d/D_A(z)$ and $r_d H(z)$, which depend on ϖ_b, ϖ_m, H_0 and T_0 in our model (see Eq. (19) and Eq. (15)). Once ϖ_b, ϖ_m are fixed by the priors, we are left with two parameters to constrain H_0 and T_0 , which allows one to eventually break the degeneracy between them. This explains why the $H_0 - T_0$ posterior contour from the BAO in Fig. 5 is not an infinite line. However, as we can see from this plot, even though the T_0 and H_0 measurements from the BAO alone are possible in principle, the resulting constraints are quite loose because the anisotropic part of the BAO signal is a very weak function of cosmological parameters. In combination with Planck only the best measured isotropic BAO part matters.

Additionally, one can constrain the peculiar velocity fluctuation r.m.s. $f\sigma_8$ from redshift-space distortions. All these pieces of information break the geometric degeneracies between the late-time parameters $\omega_{cdm}, \omega_b, h$ and T_0 .

Alternatively, one can break the geometric degeneracy and measure T_0 from the Planck data by the local measurement from SH0ES that yields a direct prior on H_0 . In this paper we will focus on these two possibilities: the BAO from galaxy surveys and local measurement of H_0 by Cepheid-calibrated supernovae.

3.8. Dependence on the calibration

Just like any bolometer, the Planck satellite measures a power output P , proportional to the electromagnetic intensity, hence temperature, as a function of direction \hat{n} . Formally (and dropping additional complexities related to the instrumental beam), we have

$$P(\hat{n}) = G \times T(t, \hat{n}) = GT_0 \left(1 + \frac{\Delta T(\hat{n})}{T_0} \right), \quad (32)$$

where G is the instrumental gain. Therefore to extract the temperature fluctuation $\Delta T(\hat{n})/T_0$, the first step is to calibrate the instrument, i.e. estimate GT_0 . The lower frequency channels of the Planck HFI instrument (100,

¹⁰ Here we use $z_{\text{eff}} = 0.38$, the effective redshift of the low- z BOSS galaxy sample [35].

143, 217, and 353 GHz), which are the most relevant for cosmological-parameter estimation, are calibrated by using the time-varying orbital dipole [54]. The basic idea is as follows: the orbital velocity $\vec{v}_{\text{orb}}(t)$ of the satellite leads to a time-varying CMB dipole in the satellite's rest frame, with temperature

$$T_{\text{orb}}(t, \hat{n}) = \hat{n} \cdot \vec{v}_{\text{orb}}(t) T_0, \quad (33)$$

leading to a time-varying power output $P_{\text{orb}}(t, \hat{n}) = GT_0(\hat{n} \cdot \vec{v}_{\text{orb}}(t))$. The orbital velocity of the satellite is very well known, and as a consequence, it is possible to determine the product GT_0 to high accuracy. Therefore, without any prior information on T_0 , Planck can accurately measure the *relative* (dimensionless) temperature fluctuation $\Delta T(\hat{n})/T_0$.

In practice, the data is provided in terms of a dimensionfull temperature power spectrum D_ℓ^{data} (with units of μK^2), under the assumption that $T_0 = T_{0,\text{FIRAS}}$, which amounts to multiplying the relative fluctuations by $T_{0,\text{FIRAS}}$. To account for this rescaling, we therefore need to multiply the dimensionless theoretical C_ℓ 's computed by CLASS by $T_{0,\text{FIRAS}}^2$:

$$D_\ell^{\text{theory}} \equiv T_{0,\text{FIRAS}}^2 \frac{\ell(\ell+1)}{2\pi} C_\ell^{\text{theory}}. \quad (34)$$

In the first version of this paper, we had incorrectly multiplied C_ℓ^{theory} by the floating T_0^2 rather than $T_{0,\text{FIRAS}}^2$. This would have been appropriate had Planck been calibrated on a source whose absolute brightness is known (such as a planet). This is indeed how the higher frequency channels are calibrated [54], but those are mostly relevant to foreground separation, and the scaling (34) is the one most adequate for cosmological parameter estimation. We explain in Appendix A why this apparently innocuous error led to artificially tighter constraints on T_0 from the Planck data alone.

4. RESULTS

We will now fit our $T_0 - \Lambda\text{CDM}$ model to cosmological data, with a flat prior on the seven parameters motivated by the previous discussion: the CMB temperature itself, T_0 , plus the six combinations that determine the CMB spectra independently of T_0 , up to the late ISW and CMB lensing effects: $\{\omega_b \hat{T}_0^{-3}, \omega_{\text{cdm}} \hat{T}_0^{-3}, \theta_s, \ln(10^{10} A_s \hat{T}_0^{n_s-1}), \tau_{\text{reio}}, n_s\}$, with $\hat{T}_0 = T_0/T_{0,\text{FIRAS}}$.

Note that in section 3.4, we argued that the quantity fixing the overall normalization of the CMB spectra independently of T_0 was $A_s T_0^{n_s-1}$. This explains why we take $\ln(10^{10} A_s \hat{T}_0^{n_s-1})$ as one of our basis parameters.

The triangle plots with posterior densities and marginalized distributions for the parameters of our $T_0 - \Lambda\text{CDM}$ model (including the derived parameter H_0) are shown in Fig. 6. For comparison, we also display the contours obtained with a baseline Planck analysis with T_0 fixed to the FIRAS prior. The results of this analysis are in good agreement with the ones reported by the Planck collaboration [4].¹¹ The marginalized limits are presented in Table I.

Let us first focus on the Planck-only results. The first relevant observation is that the posterior distribution of the parameters $\{\omega_b \hat{T}_0^{-3}, \omega_{\text{cdm}} \hat{T}_0^{-3}, \ln(10^{10} A_s \hat{T}_0^{n_s-1}), \theta_s\}$ are almost the same in the fit with free T_0 and with T_0 fixed to the FIRAS value. There are some small shifts (well below statistical uncertainties) which are produced by small residual correlations between primary and secondary effects.

We can see that releasing T_0 in the fit introduces a strong degeneracy direction $T_0 - H_0$, in line with our theoretical arguments. The resulting posterior for T_0 is very non-Gaussian and peaks at $T_0 \approx 3.3$ K, which corresponds to the region of the parameter space with $\Omega_\Lambda \approx 0$. It is worth mentioning that we have explicitly imposed a physical prior $\Omega_\Lambda \geq 0$ in our MCMC chains, translating¹² to a prior $T_0 \lesssim 3.3$ K. The skewed shape of the T_0 posterior reflects this prior. The preference for $\Omega_\Lambda = 0$ can be traced back to the anomalies of the Planck data, i.e. the low- ℓ deficit and the lensing anomaly. Remarkably, releasing T_0 allows one to fit both these anomalies simultaneously. Indeed, increasing T_0 suppresses the large-scale ISW contribution, which is preferred by the low- ℓ data. Moreover, it enhances the late-time matter clustering and the CMB lensing effect, which is preferred by the observed smoothing of the CMB peaks in the Planck

¹¹ We have found some small shifts in the cosmological parameters, which resulted from using HyRec instead of recfast [27, 55].

These shifts are very small relative to statistical uncertainties.

¹² To get this, we rewrite the condition $\Omega_\Lambda \equiv 1 - \Omega_m \geq 0$ as

$$1 \geq \omega_m h^{-2} \Rightarrow \frac{T_0}{T_{0,\text{FIRAS}}} \leq (h^2 (\omega_m \hat{T}_0^{-3})^{-1})^{1/3} \quad (35)$$

and use the best-fit values for $h \approx 0.5$ and $\omega_m \hat{T}_0^{-3} = 0.14$.

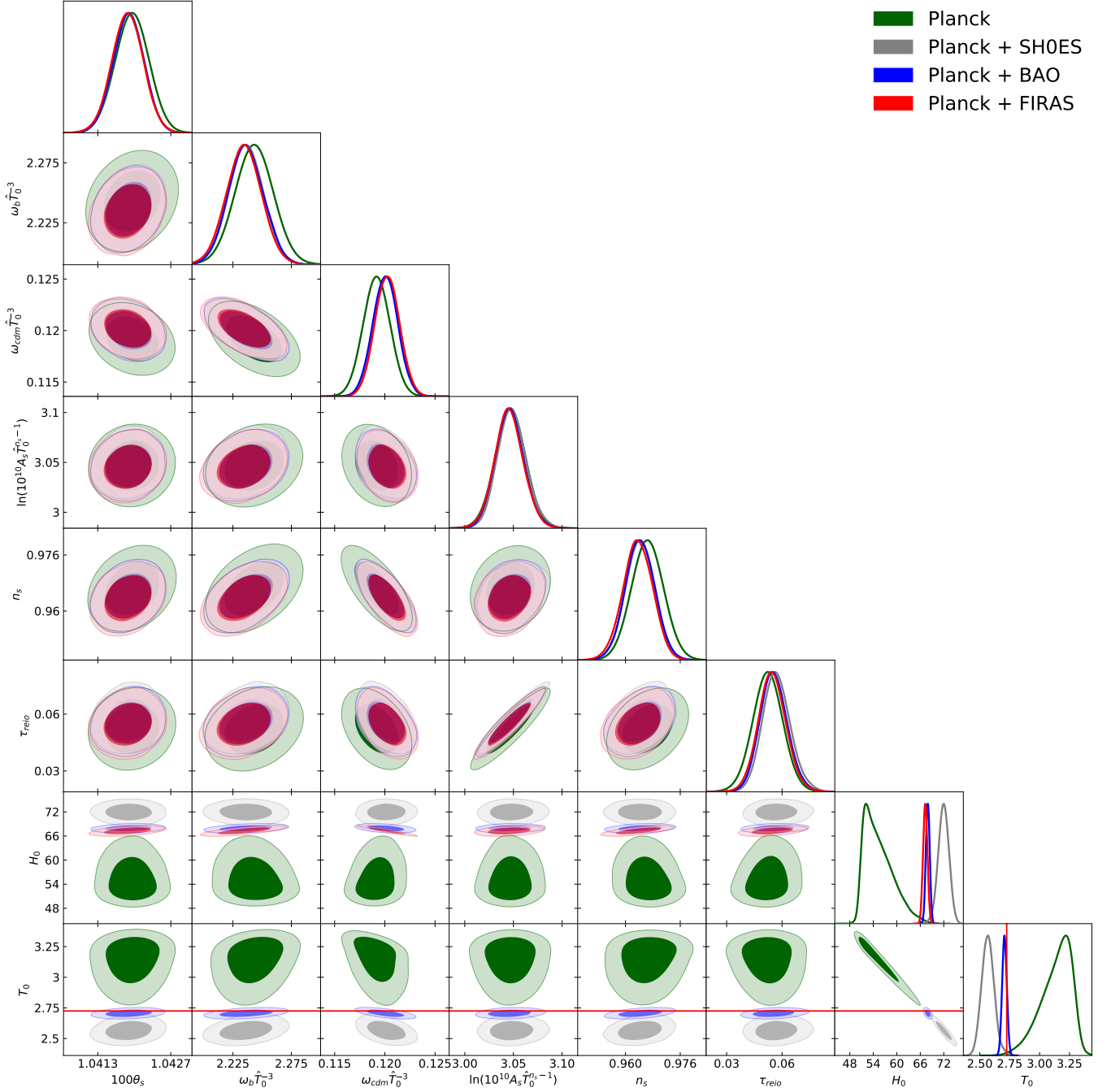


FIG. 6. Posterior distributions and marginalized 68% and 95% confidence contours for the cosmological parameters of the $T_0 - \Lambda$ CDM model fitted to Planck (in green), Planck+SH0ES (in gray), and Planck + BAO (in blue). For comparison, we also show the result of the Planck baseline analysis with T_0 fixed to the FIRAS best-fit value 2.7255 K (in red).

TT spectra¹³ We analyze the impact of these anomalies on the eventual Planck-only constraints in Appendix B.

At face value, the Planck-only posterior for T_0 is in ten-

¹³ Note that the latter effect is not fully captured by common mass fluctuation amplitude parameter σ_8 because the physical length

corresponding to the comoving scale $R = 8$ Mpc/h is different in models with different T_0 and H_0 , and thus σ_8 effectively measures the density fluctuations smoothed at different scales. When

Dataset Parameter	Planck + FIRAS	Planck	Planck + SH0ES	Planck + BAO
$100 \omega_b \hat{T}_0^{-3}$	$2.235^{+0.015}_{-0.014}$	$2.243^{+0.015}_{-0.015}$	$2.236^{+0.015}_{-0.015}$	$2.236^{+0.015}_{-0.014}$
$\omega_{cdm} \hat{T}_0^{-3}$	$0.1202^{+0.0012}_{-0.0012}$	$0.1192^{+0.0013}_{-0.0013}$	$0.1202^{+0.0012}_{-0.0012}$	$0.1200^{+0.0012}_{-0.0012}$
$100 \theta_s$	$1.0419^{+0.00029}_{-0.0003}$	$1.042^{+0.0003}_{-0.0003}$	$1.042^{+0.00029}_{-0.0003}$	$1.042^{+0.0003}_{-0.0003}$
τ_{reio}	$0.05468^{+0.0069}_{-0.0078}$	$0.05218^{+0.0075}_{-0.0076}$	$0.05695^{+0.007}_{-0.0081}$	$0.05546^{+0.0072}_{-0.0079}$
$\ln(10^{10} A_s \hat{T}_0^{n_s-1})$	$3.045^{+0.014}_{-0.015}$	$3.047^{+0.015}_{-0.015}$	$3.046^{+0.015}_{-0.015}$	$3.046^{+0.014}_{-0.015}$
n_s	$0.9637^{+0.0041}_{-0.0043}$	$0.9664^{+0.0043}_{-0.0043}$	$0.9641^{+0.0043}_{-0.0044}$	$0.9642^{+0.0043}_{-0.0043}$
T_0	$2.72548^{+0.00057}_{-0.00057}$	$3.144^{+0.17}_{-0.065}$	$2.564^{+0.049}_{-0.051}$	$2.706^{+0.019}_{-0.02}$
$100 \omega_b$	$2.235^{+0.015}_{-0.014}$	$3.458^{+0.54}_{-0.25}$	$1.865^{+0.11}_{-0.12}$	$2.189^{+0.053}_{-0.057}$
ω_{cdm}	$0.1202^{+0.0012}_{-0.0012}$	$0.1836^{+0.028}_{-0.011}$	$0.1002^{+0.0053}_{-0.0058}$	$0.1175^{+0.002}_{-0.0021}$
Ω_Λ	$0.6834^{+0.0075}_{-0.0075}$	$0.27^{+0.086}_{-0.27}$	$0.7691^{+0.023}_{-0.019}$	$0.6963^{+0.0097}_{-0.0088}$
H_0	$67.28^{+0.53}_{-0.55}$	$55.32^{+1.7}_{-4.9}$	$72.01^{+1.3}_{-1.3}$	$67.92^{+0.49}_{-0.51}$
σ_8	$0.8117^{+0.0057}_{-0.006}$	$0.6499^{+0.026}_{-0.063}$	$0.8758^{+0.022}_{-0.022}$	$0.8186^{+0.011}_{-0.011}$

TABLE I. Mean values and 68% CL minimum credible intervals for the parameters of the $T_0 - \Lambda$ CDM model fitted to Planck+FIRAS, Planck only, Planck + SH0ES, and Planck + BAO. For comparison, we also quote in the leftmost column the results obtained for the baseline Planck analysis with T_0 fixed to the FIRAS value in the leftmost column. We assumed flat priors on the first seven parameters, which are defined in the text. The last five rows show derived parameters. H_0 is quoted in km/s/Mpc, T_0 is quoted in units of Kelvin, and $\hat{T}_0 \equiv T_0/T_{0, \text{FIRAS}}$.

sion with FIRAS, and the posterior for H_0 is in tension with both Planck+FIRAS and SH0ES. Indeed, the corresponding regions of the parameter space have no overlap with the 95% CL area of the Planck-only posterior. However, there are three important observations. First, the T_0 measurement turns out to be very sensitive to statistical anomalies in the Planck data, which may pull the T_0 posterior away from the position expected in a fair sample. Second, the quantification of tensions can be subtle given a highly-skewed nature of the Planck-only probability distribution functions for H_0 and T_0 . Third, one may expect that at least part of the tension can also be driven by the Bayesian prior volume effects. Indeed, the peak of the posterior distribution for T_0 and H_0 maps onto the region $\Omega_\Lambda \simeq 0$, which hits the physical prior $\Omega_\Lambda \geq 0$ that we imposed for this parameter. It is instructive to compare the values of χ^2 at relevant best-fit points. The difference in χ^2 of the Planck-only likelihood between the Planck-only and Planck + FIRAS best-fitting points is

given by¹⁴

$$\begin{aligned} \Delta\chi^2_{\text{eff}} &= \chi^2_{\text{eff}}(\text{Planck}) - \chi^2_{\text{eff}}(\text{Planck} + \text{FIRAS}) \\ &= 2769.7 - 2775.64 = -5.94. \end{aligned} \quad (36)$$

This difference is similar to typical improvements due to a better fit of the anomalies in the Planck spectra, which can be obtained, e.g. by including the spatial curvature or the unphysical lensing smoothing parameter A_L in the Λ CDM fit [4, 27]. In this paper we adopt the point of view that these anomalies are statistical fluctuations [4, 27, 56, 57]. Therefore, in order to reduce their effect one should combine the Planck data with other data sets. Indeed, since T_0 manifests itself only through the late-time expansion effects, late-Universe probes like BAO or SH0ES will be able to efficiently break the $H_0 - T_0$ degeneracy and reduce the dependence of the Planck-only constraints on the internal anomalies. The situation here is similar to the inclusion of the BAO data in the analysis with floating curvature parameter

the Planck+FIRAS and Planck $T_0 - \Lambda$ CDM best-fit models are compared at the same fixed *energy* scales, the power spectrum amplitude is larger in the $T_0 - \Lambda$ CDM model, see Fig. 2.

¹⁴ The contributions from different likelihoods are: -4.96 (high- ℓ TTTEEE); -0.26 (low- ℓ EE); -1.72 (low- ℓ TT); $+1.0$ (lensing).

Ω_k , which allows one to remove the anomalous preference of the primary CMB data for a non-zero spatial curvature [4, 27].

The geometric degeneracy between H_0 and T_0 gets broken once we impose the H_0 prior from SH0ES. The effective χ_{eff}^2 of the Planck likelihoods computed at the best-fitting point to the Planck+SH0ES dataset is slightly worse than that of the concordance model – or in other words, than that computed at the best-fitting point to Planck+FIRAS – by:

$$\begin{aligned} \Delta\chi_{\text{eff}}^2 &\equiv \chi_{\text{eff}}^2(\text{Planck+SH0ES}) - \chi_{\text{eff}}^2(\text{Planck+FIRAS}) \\ &= 2778.82 - 2775.64 = 3.18. \end{aligned} \quad (37)$$

In the Planck+SH0ES analysis, the best-fit T_0 is significantly lower than the FIRAS value. This was to be expected from the CMB geometric degeneracy $H_0 \propto T_0^{-1.2}$, which requires a smaller T_0 in order to be consistent with the larger H_0 prior from SH0ES, given the very well constrained angle θ_s . The optimal values of T_0 from Planck + SH0ES and FIRAS are separated by $\Delta T_0 = 0.16$ K, which corresponds to 3.3 standard deviations (adding in quadrature the Planck + SH0ES and the FIRAS errors). We see that by floating T_0 , we have traded the usual 4.1σ Hubble tension¹⁵ between Planck+FIRAS and SH0ES for a 3.2σ T_0 tension between FIRAS and Planck+SH0ES.

If we use the BAO to break the geometric degeneracy instead of SH0ES, we obtain a measurement of T_0 that agrees with the FIRAS measurement within 68% CL. The goodness of fit to Planck data does not degrade much in this case,

$$\begin{aligned} \Delta\chi_{\text{eff}}^2 &\equiv \chi_{\text{eff}}^2(\text{Planck+BAO}) - \chi_{\text{eff}}^2(\text{Planck+FIRAS}) \\ &= 2776.28 - 2775.64 = 0.64. \end{aligned} \quad (38)$$

Overall, we observe good agreement between Planck+BAO and FIRAS.

In this work, for concision, we did not discuss the constraints coming from the measurement of the amplitude of the matter power spectrum near the present time. We can briefly mention that weak lensing surveys often report an estimate of the parameter combination $S_8 \equiv \sigma_8(\Omega_m/0.3)^{0.5}$, and that the degeneracy discussed

in this work is such that smaller values of T_0 lead to smaller values of S_8 . For instance, our $T_0 - \Lambda$ CDM best-fit model to Planck+SH0ES has $S_8 \simeq 0.77$, in very good agreement with KIDs and DES measurements [58–60]. Thus this model would not be disfavored on the basis of weak lensing data only – but as we explained, it is disfavoured instead by BAO and FIRAS data.

5. CONCLUSIONS

In this paper, we have given a detailed description of the effects of the CMB temperature monopole T_0 on cosmological observables, namely CMB anisotropies and large-scale structure. We have shown that cosmological background quantities and perturbations are independent of T_0 when computed at fixed baryon-to-photon and dark matter-to-photon *number ratios*, and at fixed energy scales. The *observed* CMB anisotropy still depends on T_0 because this parameter quantifies the energy scale at the present time, from which observations are carried. The leading effect of T_0 on CMB anisotropies is to change the angular diameter distance to the surface of last scattering, which is degenerate with a change of the Hubble parameter H_0 . This geometric degeneracy approximately translates to the parameter degeneracy $H_0 \propto T_0^{-1.2}$.

The standard procedure to break the CMB-anisotropy geometric degeneracy is to include the very tight T_0 measurement from FIRAS. This leads to a measurement of the Hubble parameter H_0 , with the well-known tension with the SH0ES measurement. In this work, we considered whether removing the FIRAS prior on T_0 and breaking the geometric degeneracy by different means might help alleviate the Hubble tension.

First, we showed, for the first time, that CMB anisotropy data *alone* can be used to measure T_0 and H_0 simultaneously. Indeed, the geometric degeneracy is not exact: it is broken on large angular scales by the integrated Sachs-Wolfe effect, and by gravitational lensing on small angular scales. From Planck data alone, we can estimate T_0 with $\sim 4\%$ precision, $T_0 = 3.144_{-0.065}^{+0.17}$ K (68%CL). Due to the $T_0 - H_0$ geometric degeneracy, this high optimal value for T_0 is paired with a rather low Hubble constant, $H_0 = 55.3_{-4.9}^{+1.7}$ km/s/Mpc. These values are in clear tension with both FIRAS and SH0ES, but we showed that this is driven by the fact that large T_0 / low H_0 provides a better fit to internal anomalies in

¹⁵ Computed from $H_0 = 67.4 \pm 0.5$ km/s/Mpc (68%CL) for Planck in the baseline Λ CDM model.

CMB data, namely the “lensing anomaly” and the “low- ℓ deficit”, which might just be statistical flukes. Other fundamental cosmological parameters (such as the baryon-to-photon number ratio) are mostly unaffected.

Second, rather than breaking the geometric degeneracy by including the FIRAS prior on T_0 , thus inferring H_0 , we use the SH0ES prior on H_0 to obtain, for the first time, an *independent measurement* of T_0 from Planck and SH0ES, $T_0 = 2.56 \pm 0.05$ K. This measurement is in significant (3.3σ) tension with the FIRAS measurement. Thus, the H_0 tension between (Planck + FIRAS) and SH0ES can be fully recast as a T_0 tension between (Planck + SH0ES) and FIRAS. This simple result should serve as a reminder that the fundamental culprits of tensions are not necessarily any single parameter whose measurements differ between different data sets.

One may also break the $T_0 - H_0$ geometric degeneracy by including BAO data, as was done in past analyses. In that case, one finds that the resulting T_0 is consistent with that measured by FIRAS, and the measured H_0 is in tension with SH0ES. The BAO measurement thus seems to arbitrate in favor of Planck + FIRAS, and disfavor SH0ES. Still, the Hubble tension – perhaps better named the Hubble-Penzias-Wilson tension – remains to be definitively solved.

ACKNOWLEDGMENTS

We thank Antony Lewis for pointing out our incorrect handling of T_0 in the calibration of CMB temperature maps, in the first version of this paper. We also thank Jens Chluba, Simone Ferraro, Raphael Flauger, Daniel Green, Luke Hart, Jan Hamann, Colin Hill, Carlos Martins, Alessandro Melchiorri and Yvonne Wong for their useful feedback on the first version of our paper. We are grateful to Matias Zaldarriaga and David Spergel for valuable discussions. MI is partially supported by the Simons Foundation’s Origins of the Universe program. YAH is supported by NSF grant number 1820861.

Parameter estimates presented in this paper are obtained with the CLASS Boltzmann code [40] interfaced with the Montepython MCMC sampler [30, 61]. The plots with posterior densities and marginalized limits are generated with the latest version of the `getdist` pack-

age¹⁶ [62], which is part of the CosmoMC code [63, 64].

Appendix A: Dependence of constraints on the calibration

In the first version of this paper, we had used $D_\ell^{\text{incorrect}} = T_0^2 \frac{\ell(\ell+1)}{2\pi} C_\ell^{\text{theory}}$ in lieu of Eq. (34). In this appendix we explain why this incorrect scaling leads to artificially tighter bounds on T_0 from Planck data alone.

We know that in our parameter basis, the overall amplitude of the dimensionless temperature and polarization power spectra C_ℓ^{theory} depends on the combination $\tilde{A}_s \equiv A_s T_0^{n_s-1}$ (strictly speaking, for $\ell \gtrsim 14$, it depends on the combination $\tilde{A}_s e^{-2\tau_{\text{reio}}}$, but we can consider τ_{reio} to be approximately fixed by small- ℓ polarization data). When we fit the correctly normalized spectrum $D_\ell^{\text{correct}} = T_{0,\text{FIRAS}}^2 \frac{\ell(\ell+1)}{2\pi} C_\ell^{\text{theory}}$ to the Planck data, we implicitly fix the value of \tilde{A}_s . In this case, the $T_0 - H_0$ degeneracy is only lifted by the late ISW effect and the CMB lensing effect, as mentioned in sections 3.5, 3.6. As can be seen from Figs. 3 and 4, these effects moreover have a rather mild dependence on T_0 . In particular, the dependence of the lensing deflection spectrum C_ℓ^{dd} on T_0 quickly drops at scales $\ell \gtrsim 70$. We have seen that the Planck lensing likelihood probes C_ℓ^{dd} mainly at $\ell \geq 70$, and thus, is weakly sensitive to T_0 .

Instead, when one fits to the data the incorrectly normalized spectrum $D_\ell^{\text{incorrect}}$, it is the combination $T_0^2 \tilde{A}_s$ that is tightly determined by the overall amplitude of CMB primary spectra. The lensing deflection spectrum C_ℓ^{dd} is still proportional to $\tilde{A}_s = (T_0^2 \tilde{A}_s)/T_0^2$. As a consequence, varying T_0 at fixed $T_0^2 \tilde{A}_s$ leads to an overall rescaling of the lensing deflection spectrum by T_0^{-2} . This significantly increases the impact of T_0 on the smoothing of the acoustic peaks via lensing. It also boosts the sensitivity of the Planck lensing likelihood to T_0 . These effects artificially increase the sensitivity of CMB-only data to T_0 , roughly by a factor 3.

We can make this argument more quantitative with a simple Fisher analysis, accounting for the Planck instrumental noise and angular resolution as given in Ref. [65]. The elements of the 7×7 Fisher matrix of cosmological parameters take the form $F_{ij} = \sum_\ell \partial_{\Omega_i} C_\ell \mathbf{C}_\ell^{-1} \partial_{\Omega_j} C_\ell$,

¹⁶ <https://getdist.readthedocs.io/en/latest/>

where \mathcal{C}_ℓ^{-1} is the ℓ -dependent covariance matrix of the lensed TT, TE and EE power spectra (note that for simplicity, we do not quantify here the additional sensitivity to T_0 coming from the CMB lensing likelihood, and thus do not consider the lensing deflection spectrum). The variance of parameter i is then given by $(F^{-1})_{ii}$. Note that only the elements of the Fisher matrix are additive in ℓ , but not the elements of its inverse. We show in Fig. 7 the contribution of the $T_0 - T_0$ element of the Fisher matrix per $\ln \ell$, with the two different calibration scalings. When accounting for the correct scaling, we find that the low- ℓ ISW bump and the high- ℓ lensing smoothing have roughly comparable contributions to $F_{T_0 T_0}$. With the incorrect scaling, the contribution of lensing smoothing is significantly boosted and dominates $F_{T_0 T_0}$, resulting in a significant decrease in the error bar on T_0 . Note that $\text{var}(T_0) = (F^{-1})_{T_0 T_0} \neq 1/F_{T_0 T_0}$, but the two are close for small correlations.

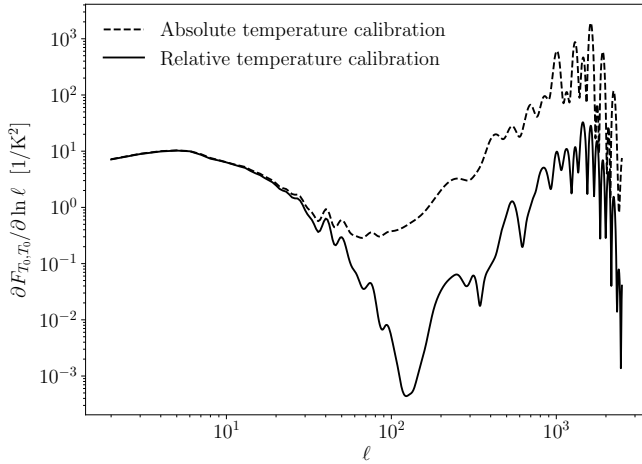


FIG. 7. Contribution of the $T_0 - T_0$ Planck Fisher matrix element per $\ln \ell$, with the correct relative calibration scaling $D_\ell = T_{0, \text{FIRAS}}^2 C_\ell$ (solid), and when incorrectly using the absolute calibration scaling $D_\ell = T_0^2 C_\ell$ (dashed). The $\ell \lesssim 10^2$ region corresponds to the ISW effect, whose contribution is mostly unaffected, and the $\ell \gtrsim 10^2$ corresponds to the lensing smoothing effect, artificially enhanced with the incorrect normalisation.

Appendix B: Quantifying different contributions in the Planck-only constraints

In this appendix we study the different contributions that form the Planck-only constraints on T_0 . Moreover,

we quantify the sensitivity of these constraints to the low- ℓ deficit and the lensing anomalies. To that end we ran three additional analyses based on Planck-only data, which we compare with the baseline case called here “low- ℓ + high- ℓ + lensing”:

1. The case “ τ -prior + high- ℓ + lensing” includes all data from Planck except the two low- ℓ (TT, EE) likelihoods, which cover $\ell \leq 29$. Since these low- ℓ likelihoods are the only ones constraining τ_{reio} , we add to this data set a Gaussian prior $\tau_{\text{reio}} = 0.0544 \pm 0.075$; however any information on the low- ℓ deficit and on the late ISW effect is removed.
2. The case “low- ℓ + high- ℓ ” includes all data from Planck except the lensing likelihood derived from 4-point correlation functions. CMB lensing is then only probed through the smoothing of the TT, TE, EE spectra.
3. The case “low- ℓ + high- ℓ + A_L ” includes the same data (all Planck data except the lensing likelihood) and features one additional and unphysical parameter A_L , that rescales the lensing deflection spectrum, and thus parametrizes the amplitude of the smoothing of the acoustic peaks due to CMB lensing.

The comparison of the first case with the baseline is intended to isolate the impact of the late-time ISW effect. The comparison of the second case with the baseline isolates the impact of CMB lensing, as probed by the measurement of the lensing deflection spectrum with the 4-point correlation functions. Finally, the comparison of the second and third case is aimed to isolate to some extent the impact of CMB lensing as probed instead by the smoothing of the TT, TE and EE spectra. The results of our analyses are summarized in Table II and in Fig. 8.

The comparison of the first case with the baseline (orange versus green curves) confirms that the late ISW effect contributes to the preference for a large T_0 , since the 68% lower bound on T_0 increases by 0.046K (i.e. by about $\sim 0.6\sigma$) when the low- ℓ data is restored. We have seen that a large T_0 implies a lower ISW component in the temperature spectrum, and thus provides a better fit to the low- ℓ data (in particular, to the low quadrupole). However, without low- ℓ data, there is still a clear preference for a large $T_0 = 3.110^{+0.20}_{-0.077}$ K (68%CL, orange curve), suggesting that the deficit in the low- ℓ data is not

the main effect that pushes T_0 above the standard value. We get an independent confirmation of this conclusion when comparing the likelihood of the best-fit Λ CDM and Λ CDM+ T_0 models, both fitted to the full Planck baseline data. Out of the total $\Delta\chi^2 \approx -6$ reported in eq. (36), only $\Delta\chi^2 \approx -2$ comes from the two low- ℓ likelihoods. This suggests that the late ISW effect and the low- ℓ deficit contribute by only $\sim 30\%$ to the preference for a large T_0 . Since T_0 impacts CMB data only through the late ISW and CMB lensing effects, the remaining 70% can either be driven by (i) the measurement of the lensing deflection spectrum, or (ii) the smoothing of the acoustic peak in the TT, TE, EE spectra.

To evaluate the impact of the former, we can compare the second case with the baseline results (purple versus green curves). Actually, when the lensing likelihood is removed, the preference for a high T_0 is stronger: the 68% lower bound on T_0 increases by 0.056K (i.e. by about $\sim 0.8\sigma$). This suggests that the lensing spectrum data prefers standard values of T_0 , and thus, the lensing smoothing must be the main effect responsible for the large T_0 preference. Once more, this can be confirmed by the comparison of the likelihood of the best-fit Λ CDM and Λ CDM+ T_0 models, both fitted to the full Planck baseline data. The best fit model of the extended case slightly degrades the lensing likelihood by $\Delta\chi^2 \approx +1$, while it improves the high- ℓ likelihood by $\Delta\chi^2 \approx -5$. Looking at the impact of T_0 on C_ℓ^{dd} (see figure 4), we conclude that Planck data on the extracted lensing spectrum does not favor the enhancement of the peak caused by large values of T_0 .

Since large T_0 values are driven by the high- ℓ likelihood, which is only sensitive to T_0 through lensing smoothing effects, there must be a strong connection between the preference for a large T_0 and the well-known “lensing anomaly”, i.e. that fact that high- ℓ Planck data can be better fitted when assuming a larger lensing smoothing effect than that predicted by the concordance Λ CDM model. It is thus interesting to compare cases two and three, which contain the same amount of Planck data (i.e. everything except the lensing likelihood), but differ through the floating of the A_L parameter. If the effect of A_L and T_0 were exactly equivalent, and if T_0 was left totally free, we would expect the Λ CDM+ T_0 + A_L model to be fully compatible with $A_L = 1$, and to fit the high- ℓ likelihood as well as the Λ CDM+ A_L model. This is not exactly the case because the prior $\Omega_\Lambda > 0$ implies a cut

around $T_0 < 3.3\text{K}$ that prevents T_0 to account for the full effect of $A_L = 1.19$ (which is the best-fit value for this data set). The shape of the T_0 posterior suggests that without the prior $\Omega_\Lambda > 0$, T_0 would be driven to even higher values, and would produce even more lensing smoothing. As a result, in the Λ CDM+ T_0 + A_L fit, A_L remains larger than one (but the physical value $A_L = 1$ is now in 1.7σ agreement with the data). Another way to see this is that the best-fit Λ CDM+ T_0 model fitted to the “low- ℓ + high- ℓ ” data reduces the χ^2 of the high- ℓ likelihood by $\Delta\chi^2 \approx -5$, while with the same data, the best-fit Λ CDM+ A_L model reduces it by $\Delta\chi^2 \approx -7.5$ (section 3.7 of [66]). In the Λ CDM+ T_0 + A_L fit, T_0 is more compatible with the FIRAS value than when A_L is fixed to one, but larger values of T_0 are still preferred; this comes from a volume effect in the marginalization of the T_0 posterior over A_L , bearing in mind that in this fit, the role of increasing the lensing smoothing effect is shared between the two parameters A_L and T_0 .

As a final comment, we note that the Λ CDM+ T_0 model (which is physical, although in strong tension with direct T_0 measurements) does a better job in fitting the full Planck data than the Λ CDM+ A_L model (which is unphysical). This comes from the fact that T_0 increases the lensing deflection spectrum only on large scales (see figure 4), while A_L increases it on all scales. Large values of both parameters are favored because they produce more smoothing in the TT, TE, EE spectrum (the smoothing depends mainly on the amplitude of C_ℓ^{dd} around the peak), but large values of A_L are more penalised by the lensing likelihood. Indeed, this likelihood is sensitive to C_ℓ^{dd} on smaller angular scales – at which the effect of A_L is clearly disfavored while T_0 has a smaller no impact. Again this can be seen very well by comparing best-fit χ^2 ’s. When the Λ CDM+ A_L is fitted to the full Planck data, it reduces the best-fit χ^2 by only -3.4 (section 3.39 of [66]), because large values of A_L are strongly penalized by the lensing likelihood. Instead, the Λ CDM+ T_0 model reduces the best-fit χ^2 by -6 because large values of T_0 are less penalized by the lensing likelihood.

Overall, the observed trends suggest the following picture: the bias of T_0 toward high values is driven by the Planck high- ℓ likelihood and can be partly understood as a result of the “lensing anomaly.” This shift also produces a better fit to the low- ℓ data. The only data set that pulls T_0 (and H_0) in the opposite direction toward

the Planck+FIRAS concordance model is the CMB lensing reconstruction data.

-
- [1] A. G. Riess, S. Casertano, W. Yuan, L. M. Macri, and D. Scolnic, *Astrophys. J.* **876**, 85 (2019), [arXiv:1903.07603 \[astro-ph.CO\]](#).
 - [2] M. J. Reid, D. W. Pesce, and A. G. Riess, *Astrophys. J.* **886**, L27 (2019), [arXiv:1908.05625 \[astro-ph.GA\]](#).
 - [3] K. C. Wong *et al.*, (2019), [arXiv:1907.04869 \[astro-ph.CO\]](#).
 - [4] N. Aghanim *et al.* (Planck), (2018), [arXiv:1807.06209 \[astro-ph.CO\]](#).
 - [5] T. M. C. Abbott *et al.* (DES), *Mon. Not. Roy. Astron. Soc.* **480**, 3879 (2018), [arXiv:1711.00403 \[astro-ph.CO\]](#).
 - [6] A. Cuceu, J. Farr, P. Lemos, and A. Font-Ribera, (2019), [arXiv:1906.11628 \[astro-ph.CO\]](#).
 - [7] N. Schöneberg, J. Lesgourgues, and D. C. Hooper, (2019), [arXiv:1907.11594 \[astro-ph.CO\]](#).
 - [8] M. M. Ivanov, M. Simonovic, and M. Zaldarriaga, (2019), [arXiv:1909.05277 \[astro-ph.CO\]](#).
 - [9] G. D’Amico, J. Gleyzes, N. Kokron, D. Markovic, L. Senatore, P. Zhang, F. Beutler, and H. Gil-Marín, (2019), [arXiv:1909.05271 \[astro-ph.CO\]](#).
 - [10] T. Colas, G. D’amico, L. Senatore, P. Zhang, and F. Beutler, (2019), [arXiv:1909.07951 \[astro-ph.CO\]](#).
 - [11] O. H. Philcox, M. M. Ivanov, M. Simonović, and M. Zaldarriaga, [arXiv:2002.04035 \[astro-ph.CO\]](#).
 - [12] E. Aubourg *et al.*, *Phys. Rev. D* **92**, 123516 (2015), [arXiv:1411.1074 \[astro-ph.CO\]](#).
 - [13] P. Lemos, E. Lee, G. Efstathiou, and S. Gratton, *Mon. Not. Roy. Astron. Soc.* **483**, 4803 (2019), [arXiv:1806.06781 \[astro-ph.CO\]](#).
 - [14] M. Rigault *et al.*, *Astrophys. J.* **802**, 20 (2015), [arXiv:1412.6501 \[astro-ph.CO\]](#).
 - [15] C. S. Kochanek, (2019), [arXiv:1911.05083 \[astro-ph.CO\]](#).
 - [16] K. Blum, E. Castorina, and M. Simonović, (2020), [arXiv:2001.07182 \[astro-ph.CO\]](#).
 - [17] L. Knox and M. Millea, (2019), [arXiv:1908.03663 \[astro-ph.CO\]](#).
 - [18] D. J. Fixsen, E. S. Cheng, J. M. Gales, J. C. Mather, R. A. Shafer, and E. L. Wright, *Astrophys. J.* **473**, 576 (1996), [arXiv:astro-ph/9605054 \[astro-ph\]](#).
 - [19] D. J. Fixsen, *Astrophys. J.* **707**, 916 (2009), [arXiv:0911.1955 \[astro-ph.CO\]](#).
 - [20] H. P. Gush, M. Halpern, and E. H. Wishnow, *Phys. Rev. Lett.* **65**, 537 (1990).
 - [21] P. Noterdaeme, P. Petitjean, R. Srianand, C. Ledoux, and S. López, *Astron. Astrophys.* **526**, L7 (2011), [arXiv:1012.3164 \[astro-ph.CO\]](#).
 - [22] A. Kogut *et al.*, *JCAP* **07**, 025 (2011), [arXiv:1105.2044 \[astro-ph.CO\]](#).
 - [23] M. H. Abitbol, J. Chluba, J. C. Hill, and B. R. Johnson, *Mon. Not. Roy. Astron. Soc.* **471**, 1126 (2017), [arXiv:1705.01534 \[astro-ph.CO\]](#).
 - [24] J. Chluba and R. A. Sunyaev, *Astron. Astrophys.* (2007), 10.1051/0004-6361:20078200, [*Astron. Astrophys.*478,L27(2008)], [arXiv:0707.0188 \[astro-ph\]](#).
 - [25] J. Hamann and Y. Y. Y. Wong, *JCAP* **0803**, 025 (2008), [arXiv:0709.4423 \[astro-ph\]](#).
 - [26] J. Yoo, E. Mitsou, Y. Dirian, and R. Durrer, *Phys. Rev. D* **100**, 063510 (2019), [arXiv:1905.09288 \[astro-ph.CO\]](#).
 - [27] P. A. R. Ade *et al.* (Planck), *Astron. Astrophys.* **594**, A13 (2016), [arXiv:1502.01589 \[astro-ph.CO\]](#).
 - [28] E. Di Valentino *et al.* (CORE), *JCAP* **1804**, 017 (2018), [arXiv:1612.00021 \[astro-ph.CO\]](#).
 - [29] M. H. Abitbol, J. C. Hill, and J. Chluba, (2019), 10.3847/1538-4357/ab7b70, [arXiv:1910.09881 \[astro-ph.CO\]](#).
 - [30] T. Brinckmann and J. Lesgourgues, (2018), [arXiv:1804.07261 \[astro-ph.CO\]](#).
 - [31] N. Aghanim *et al.* (Planck), (2019), [arXiv:1907.12875 \[astro-ph.CO\]](#).
 - [32] S. Seager, D. D. Sasselov, and D. Scott, *Astrophys. J.* **523**, L1 (1999), [arXiv:astro-ph/9909275 \[astro-ph\]](#).
 - [33] Y. Ali-Haïmoud and C. M. Hirata, *Phys. Rev. D* **82**, 063521 (2010), [arXiv:1006.1355 \[astro-ph.CO\]](#).
 - [34] Y. Ali-Haïmoud and C. M. Hirata, *Phys. Rev. D* **83**, 043513 (2011), [arXiv:1011.3758 \[astro-ph.CO\]](#).
 - [35] S. Alam *et al.* (BOSS), *Mon. Not. Roy. Astron. Soc.* **470**, 2617 (2017), [arXiv:1607.03155 \[astro-ph.CO\]](#).
 - [36] A. Chudaykin, M. M. Ivanov, and M. Simonović, (2020), [arXiv:2004.10607 \[astro-ph.CO\]](#).
 - [37] M. M. Ivanov, M. Simonović, and M. Zaldarriaga, (2019), [arXiv:1912.08208 \[astro-ph.CO\]](#).
 - [38] H. du Mas des Bourboux *et al.*, *Astron. Astrophys.* **608**, A130 (2017), [arXiv:1708.02225 \[astro-ph.CO\]](#).
 - [39] M. Ata *et al.*, *Mon. Not. Roy. Astron. Soc.* **473**, 4773 (2018), [arXiv:1705.06373 \[astro-ph.CO\]](#).
 - [40] D. Blas, J. Lesgourgues, and T. Tram, *JCAP* **1107**, 034 (2011), [arXiv:1104.2933 \[astro-ph.CO\]](#).
 - [41] W. Hu, ASP Conf. Ser. **339**, 215 (2005), [arXiv:astro-ph/0407158](#).
 - [42] W. T. Hu, *Wandering in the Background: A CMB Explorer*, Other thesis (1995), [arXiv:astro-ph/9508126](#).
 - [43] C.-P. Ma and E. Bertschinger, *Astrophys. J.* **455**, 7 (1995), [arXiv:astro-ph/9506072 \[astro-ph\]](#).
 - [44] D. S. Gorbunov and V. A. Rubakov, *Introduction to the*

Dataset Parameter	Planck + FIRAS	low ℓ +high ℓ +lens.	high ℓ +lens.+ τ	low ℓ +high ℓ	low ℓ +high ℓ + A_L
$100\omega_b\hat{T}_0^{-3}$	$2.235^{+0.015}_{-0.014}$	$2.243^{+0.015}_{-0.015}$	$2.243^{+0.015}_{-0.015}$	$2.242^{+0.015}_{-0.015}$	$2.256^{+0.017}_{-0.017}$
$\omega_{cdm}\hat{T}_0^{-3}$	$0.1202^{+0.0012}_{-0.0012}$	$0.1192^{+0.0013}_{-0.0013}$	$0.1192^{+0.0013}_{-0.0013}$	$0.1196^{+0.0013}_{-0.0013}$	$0.1183^{+0.0015}_{-0.0015}$
$100\theta_s$	$1.0419^{+0.00029}_{-0.0003}$	$1.042^{+0.0003}_{-0.0003}$	$1.042^{+0.00031}_{-0.0003}$	$1.042^{+0.0003}_{-0.0003}$	$1.042^{+0.00031}_{-0.00031}$
τ_{reio}	$0.05468^{+0.0069}_{-0.0078}$	$0.05218^{+0.0075}_{-0.0076}$	$0.05533^{+0.0071}_{-0.0071}$	$0.05412^{+0.0077}_{-0.0076}$	$0.0507^{+0.0086}_{-0.0079}$
$\ln(10^{10}A_s\hat{T}_0^{n_s-1})$	$3.045^{+0.014}_{-0.015}$	$3.047^{+0.015}_{-0.015}$	$3.052^{+0.013}_{-0.013}$	$3.053^{+0.016}_{-0.016}$	$3.042^{+0.017}_{-0.017}$
n_s	$0.9637^{+0.0041}_{-0.0043}$	$0.9664^{+0.0043}_{-0.0043}$	$0.9658^{+0.0046}_{-0.0044}$	$0.9655^{+0.0045}_{-0.0044}$	$0.9695^{+0.005}_{-0.0051}$
T_0	$2.72548^{+0.00057}_{-0.00057}$	$3.144^{+0.17}_{-0.065}$	$3.110^{+0.2}_{-0.077}$	$3.195^{+0.011}_{-0.06}$	$3.162^{+0.16}_{-0.063}$
A_L	—	—	—	—	$1.119^{+0.063}_{-0.07}$
$100\omega_b$	$2.235^{+0.015}_{-0.014}$	$3.458^{+0.54}_{-0.25}$	$3.355^{+0.64}_{-0.29}$	$3.623^{+0.38}_{-0.25}$	$3.538^{+0.54}_{-0.25}$
ω_{cdm}	$0.1202^{+0.0012}_{-0.0012}$	$0.1836^{+0.028}_{-0.011}$	$0.1782^{+0.034}_{-0.013}$	$0.1932^{+0.02}_{-0.0081}$	$0.1854^{+0.028}_{-0.011}$
Ω_Λ	$0.6834^{+0.0075}_{-0.0075}$	$0.27^{+0.086}_{-0.27}$	$0.31^{+0.17}_{-0.23}$	$0.19^{+0.08}_{-0.17}$	$0.25^{+0.085}_{-0.25}$
H_0	$67.28^{+0.53}_{-0.55}$	$55.32^{+1.7}_{-4.9}$	$56.29^{+2}_{-5.8}$	$55.36^{+1.3}_{-3.2}$	$55.26^{+1.7}_{-4.7}$
σ_8	$0.8117^{+0.0057}_{-0.006}$	$0.6499^{+0.026}_{-0.063}$	$0.6645^{+0.029}_{-0.075}$	$0.6325^{+0.024}_{-0.042}$	$0.6409^{+0.025}_{-0.059}$

TABLE II. Mean values and 68% CL minimum credible intervals for the parameters of the $T_0 - \Lambda$ CDM model fitted to various data sets: low- ℓ + high- ℓ + lensing, τ -prior+high- ℓ [$\ell \geq 30$]+lensing, low- ℓ +high- ℓ , low- ℓ +high- ℓ +free A_L , and full Planck (low- ℓ + high- ℓ + lensing)+FIRAS, see the main text for more detail. We assumed flat priors on the first seven parameters, which are defined in the text. The last five rows show derived parameters. H_0 is quoted in km/s/Mpc, T_0 is quoted in units of Kelvin, and $\hat{T}_0 \equiv T_0/T_{0,\text{FIRAS}}$.

theory of the early universe: Cosmological perturbations and inflationary theory (2011).

- [45] A. Lewis and A. Challinor, *Phys. Rept.* **429**, 1 (2006), [arXiv:astro-ph/0601594 \[astro-ph\]](#).
- [46] C. Alcock and B. Paczynski, *Nature* **281**, 358 (1979).
- [47] T. Matsubara and Y. Suto, *Astrophys. J.* **470**, L1 (1996), [arXiv:astro-ph/9604142](#).
- [48] W. Ballinger, J. Peacock, and A. Heavens, *Mon. Not. Roy. Astron. Soc.* **282**, 877 (1996), [arXiv:astro-ph/9605017](#).
- [49] X. Xu, A. J. Cuesta, N. Padmanabhan, D. J. Eisenstein, and C. K. McBride, *Mon. Not. Roy. Astron. Soc.* **431**, 2834 (2013), [arXiv:1206.6732 \[astro-ph.CO\]](#).
- [50] A. Heinesen, C. Blake, Y.-Z. Li, and D. L. Wiltshire, *JCAP* **1903**, 003 (2019), [arXiv:1811.11963 \[astro-ph.CO\]](#).
- [51] A. Heinesen, C. Blake, and D. L. Wiltshire, *JCAP* **2001**, 038 (2020), [arXiv:1908.11508 \[astro-ph.CO\]](#).
- [52] A. L. Coil *et al.* (DEEP2 Survey), *Astrophys. J.* **609**, 525 (2004), [arXiv:astro-ph/0305586 \[astro-ph\]](#).
- [53] M. Davis, M. J. Geller, and J. Huchra, *Astrophys. J.* **221**, 1 (1978).
- [54] R. Adam *et al.* (Planck), *Astron. Astrophys.* **594**, A8 (2016), [arXiv:1502.01587 \[astro-ph.CO\]](#).
- [55] J. R. Shaw and J. Chluba, *Mon. Not. Roy. Astron. Soc.* **415**, 1343 (2011), [arXiv:1102.3683 \[astro-ph.CO\]](#).
- [56] G. Addison, Y. Huang, D. Watts, C. Bennett, M. Halpern, G. Hinshaw, and J. Weiland, *Astrophys. J.* **818**, 132 (2016), [arXiv:1511.00055 \[astro-ph.CO\]](#).
- [57] N. Aghanim *et al.* (Planck), *Astron. Astrophys.* **607**, A95 (2017), [arXiv:1608.02487 \[astro-ph.CO\]](#).
- [58] A. Drlica-Wagner *et al.* (DES), *Astrophys. J. Suppl.* **235**, 33 (2018), [arXiv:1708.01531 \[astro-ph.CO\]](#).
- [59] A. H. Wright *et al.*, *Astron. Astrophys.* **632**, A34 (2019), [arXiv:1812.06077 \[astro-ph.CO\]](#).
- [60] M. Asgari *et al.*, *Astron. Astrophys.* **634**, A127 (2020), [arXiv:1910.05336 \[astro-ph.CO\]](#).
- [61] B. Audren, J. Lesgourgues, K. Benabed, and S. Prunet, *JCAP* **1302**, 001 (2013), [arXiv:1210.7183 \[astro-ph.CO\]](#).
- [62] A. Lewis, (2019), [arXiv:1910.13970 \[astro-ph.IM\]](#).
- [63] A. Lewis and S. Bridle, *Phys. Rev.* **D66**, 103511 (2002), [arXiv:astro-ph/0205436 \[astro-ph\]](#).
- [64] A. Lewis, *Phys. Rev.* **D87**, 103529 (2013), [arXiv:1304.4473 \[astro-ph.CO\]](#).
- [65] The Planck Collaboration, *arXiv e-prints*, astro-ph/0604069 (2006), [arXiv:astro-ph/0604069 \[astro-ph\]](#).
- [66] “Planck 2018: Cosmological parameter tables,” <http://https://wiki.cosmos.esa.int/>

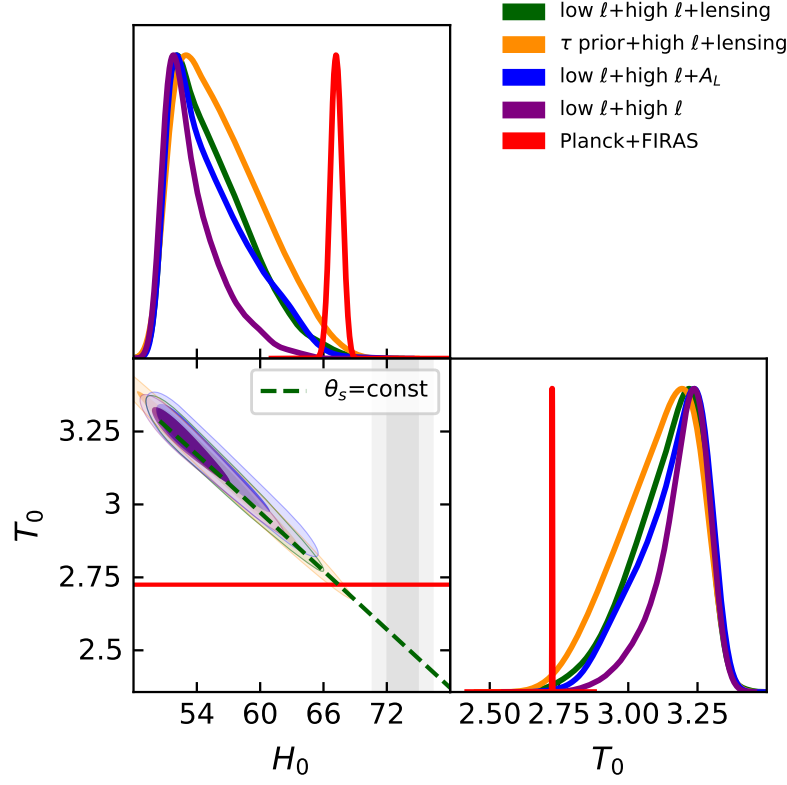


FIG. 8. Posterior distribution for T_0 and H_0 extracted from the analysis of the following Planck data sets: low- ℓ +high- ℓ +lensing, τ -prior+high- ℓ [$\ell \geq 30$]+lensing, low- ℓ +high- ℓ , low- ℓ +high- ℓ +free A_L , and full Planck (low- ℓ +high- ℓ +lensing)+FIRAS, see the main text for more detail. A horizontal solid red line marking the FIRAS value is put for illustrative purposes. The green dashed line shows the degeneracy direction $\theta_s(H_0, T_0) = \text{const}$, the vertical gray band displays the SH0ES H_0 prior.

planck-legacy-archive/images/2/21/Baseline_

[params_table_2018_95pc_v2.pdf](#).